國立臺灣大學理學院地質科學研究所

碩士論文

Department of Geosciences

College of Science

National Taiwan University

Master Thesis

由中國重慶羊口洞石筍氧同位素記錄探討過去 12 萬至

21 萬年間亞洲季風強度的變化

Asian monsoon variability during 124-206 ka inferred

from oxygen isotope records of stalagmites from Yangkou

Cave, Chongqing, China

黃莉容

Li-Jung Huang

指導教授：沈川洲 博士

Advisor: Chuan-Chou Shen, Ph.D.

中華民國 101 年 8 月

August 2012

臺灣大學碩士學位論文
口試委員會審定書

由中國重慶羊口洞石筍氧同位素記錄探討過去 12 萬至 21 萬年間亞洲季風強度的變化

Asian monsoon variability during 124-206 ka inferred from oxygen isotope records of stalagmites from Yangkou Cave, Chongqing, China

本論文係黃莉容君（R98224109）在國立臺灣大學理學院地質科學系暨研究所完成之碩士學位論文，於民國 101 年 7 月 25 日承下列考試委員審查通過及口試及格，特此證明

口試委員：

_____ （簽名）
（指導教授）

_____

_____

_____

系主任（所長）_____ （簽名）

序言與謝誌

手拿地質鎚，頭戴安全帽，僅依靠著探照燈的微弱光源，我們一步一腳印，緩緩走入那未知的深邃世界…，如果你問我兩年來的碩士心路歷程當中，哪件事令我印象最為深刻，一定沒有比在伸手不見五指的石灰岩洞穴中親自採樣更好的答案的了。如今我的論文得以順利完成，首要感謝我的**指導教授沈川洲老師**，不論是衝鋒陷陣的樣本採集，或是精細的實驗方法與儀器操作，一直到論文的撰寫與修改，您都親自帶領與指導，應該沒有比您更酷又更有耐心的教授了吧！

這篇論文的催生，也不乏許多貴人及合作對象的鼎力相助，感謝遠在重重慶的**李廷勇教授**與**楊勳林教授**在野外採樣及樣品處理與測量上所提供的協助，還有臺灣師範大學的**米泓生教授**在氧同位素測量上提供的協助，以及我的口試委員**劉平妹教授**、**陳明德教授**跟其他系上老師、學長姊還有同儕的意見提供。

「埋頭研究兩年歲月，只為畢業一只文憑」這是不少人對研究生的看法，然而從碩論研究中，我認為自己不僅僅得到了那一張畢業證書，更獲得豐富與廣闊的知識與經驗，還有獨立處理問題的能力。謝謝我的**父母與家人**，雖然你們可能沒辦法完全了解我的研究與我所走過的路，卻還是在我唸研究所且沒有謀生能力的這段期間默默地背後支持我、包容我，現在，我能夠很爭氣地告訴你們，你們的女兒在研究所歷程中獲得的，遠比一張碩士文憑多得多，希望這樣的我，並沒有令你們感到失望。

即便身處實驗室，並非只有孤獨的研究歷程伴隨著我，我的同窗好友**於蓁**陪我一起走過了這一段外人難以深刻體會的研究所生涯，**忠哲學長**一直以來的費心

教學與指導，**羅立學長**、**志凱學長**以及**韻熔**總是義不容辭地與我討論及提供各種意見，**聖菩**曾經在我出地調導論時臨時幫忙找到研究室的重要資料，**晉平**、**皓正**與**建儒**三位學弟總是擔任我們這些碩二生忙到不可開交時的救火隊，至於兩位助理 **Coco** 與**怡綺**則將我們實驗室整頓與打理得如此完善（當然也不會忘記還有前助理 **O-John** 啦～～ 怎麼可能忘記你呢：P），還有生科院的**佩萱學姊**總是貼心且適時地給我鼓勵，許多親朋好友則陪我渡過了一個又一個歡笑時光與低潮時期。因為有你們，我才能堅定地走完這辛苦的碩士歷程，回頭看看，我們所共同擁有的，那一件又一件刁鑽事項或瘋狂趣事，想必還是成就大於沮喪、歡笑大於淚水，有你們真好！

夏末秋初八月底，恰巧與我初來這個實驗室報到的時間一模一樣，縱使此時此刻蟬鳴聲不再如同畢業季時響徹雲霄，鳳凰花也早已盛開又凋零，然而當初拖著輕輕如也的行李箱來前來的我，現在卻是紮紮實實地滿載而歸。完整的兩年過去，前往下一站的列車鈴聲逐漸響起，相信帶著成就了這本碩士論文的心，我會在接下來的旅程中，一步一腳印繼續刻劃出屬於我的人生，Fight！

最後，以下送給我們實驗室即看到這本論文的你們，第一句這樣寫是因為我來報到的前一天實驗室燒掉了，但我依然準時畢業了唷～～ 所以，共勉之。此外，這也是個文字遊戲唷！能找到這其中的小小奧秘嗎？≧▽≦

初入實驗室　畢力同心　清火場
鑽研學問間　課業繁重　長知識
漫步研究裡　苦水超多　增經驗
成就此論文　秋高氣爽　得收穫

Abstract

Asian monsoon (AM) variation over past 380 kyrs has been reconstructed using stalagmite oxygen isotope records from caves in China, showing that AM intensity primarily follows Northern Hemisphere summer insolation on orbital timescales. However, those 100s-kyr records were built with stalagmites mainly from Sanbao Cave only, which could bring uncertainty in interpreting long-term AM evolution. Oxygen isotope records of stalagmites with high uranium levels of 2-16 ppm, collected from Yangkou Cave were used to reconstruct AM record from 124 to 206 kyr BP. Our results show that the Yangkou stalagmite-inferred AM variation superimposes on Sanbao record, supporting the strong AM intervals at marine isotope stage (MIS) 6.3, 6.5, and 7.1 and weak AM intervals at MIS 6.2, 6.4, and 7.0. This consistency confirms that the AM events are dominant in the entire mainland and primarily follow Northern Hemisphere summer insolation and relate to the atmospheric $\delta^{18}O$ variation on orbital timescales. Combined with Pacific thermal conditions, our study suggests that AM evolution could be partially controlled by the Walker Circulation. The conflict between stalagmite-inferred and loess-inferred Asian monsoon records during MIS 6 might be caused by the migration of Asian summer monsoon boundary. Advantages of high precision absolute U/Th dates with 2-sigma error as low as only ±450 yrs allow us to precisely determine the event durations and timings and to understand the AM variability and climatic forcings during MIS 6-7.

摘要

透過分析中國洞穴石筍氧同位素記錄，前人研究已將過去 38 萬年來的亞洲季風強弱變化重建，並顯示在天文軌道週期的時間尺度上，亞洲季風強度主要跟隨北半球夏季日照量而改變。然而，在十萬年以前的中國洞穴石筍氧同位素記錄幾乎僅來自於湖北省的三寶洞，此單一的數據可能對於亞洲季風演化過程的解釋造成些許不確定。透過分析來自重慶市的羊口洞的五支鈾濃度介於 2-16 ppm 的高鈾濃度石筍，我們利用其氧同位素和定年紀錄，重建了 12.4 萬至 20.6 萬年前的亞洲季風變化。此研究結果支持三寶洞在此時間段的亞洲季風研究成果，包含深海氧同位素階層(MIS) 6.3、6.5 與 7.1 的強季風時期，以及 MIS 6.2、6.4 與 7.0 的弱季風時期。中國洞穴石筍氧同位素變化的一致性說明過去亞洲季風興衰支配整個中國大陸地區，在天文軌道週期的時間尺度上主要跟隨北半球夏季日照量而改變，並且與全球大氣中氧氣的氧同位素變化有相關性存在。透過中國洞穴石筍氧同位素記錄與太平洋海表溫資料的對比，我們的研究提出亞洲季風的發展可能部分受控於沃克環流的強弱。前人研究顯示在 MIS 6 時期，中國洞穴石筍氧同位素記錄與黃土磁感率在季風興衰的分析上有所衝突，我們則認為此一現象是中國夏季季風系統與西北界線的遷移所造成。利用高精度的鈾釷定年技術，在 95%信賴區間（2-sigma）內，我們所分析的羊口洞的石筍定年誤差可達到僅±450 年，可讓我們更加確信在 MIS 6-7 時期亞洲季風事件的持續時間與確切的發生時間，進一步理解此時期亞洲季風的強弱變化與氣候上的影響因素。

Content

List of Figures

List of Tables

Chapter 1 Introduction

1.1 Asian monsoon

East Asia is the most densely populated areas around the world, and in this region the intensity of Asian monsoon (AM) precipitation strongly dominates regional vegetation, agriculture, culture, economy, and dynasty alternation. AM is composed of the East Asian monsoon (EAM) and South Asian monsoon (SAM), and winter monsoon generated by the Siberian-Mongolia high (Fig. 1-1) (An, 2000; Zhao et al., 2010).
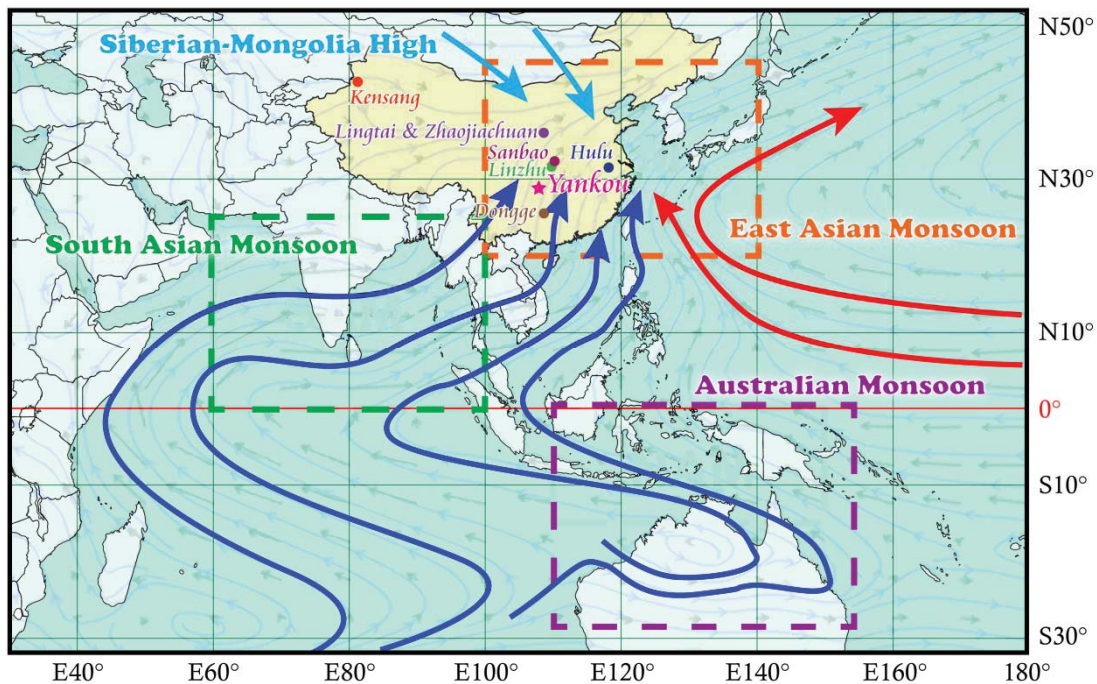
Fig. 1-1 The air flows and the relationship among three subsystems, EAM, SAM, and AUM, of Asian-Australian monsoon system.

AM climate is characterized with prominent seasonal changes in wind direction,

rainfall and temperature between cold-and-dry winter and hot-and-humid summer. The

AM circulation is not only closely associated with climatic feature of the northern high

latitudes but also linked with the equatorial ocean and the southern hemisphere

including the climatic region of the SAM and the Australian monsoon (AUM) (An,

2000). In austral summer (January), Siberian high, migrating southward, enhances

low-latitude moisture and heat to summer AUM territory by cross-equatorial transport.

In boreal summer (July), the southeasterly trade wind of north Australia migrates

northward, passes the equator, and changes the direction and becomes the southwesterly

wind, which enhances Asian Summer Monsoon (ASM) (An, 2000). An (2000)

described this relations as "pressure push" and "thermal pull" between AM in north

hemisphere (NH) and AUM in south hemisphere (SH) (Fig. 1-2) (An, 2000).
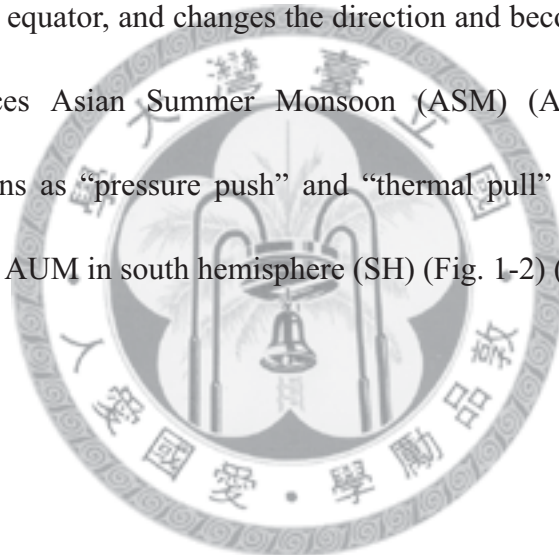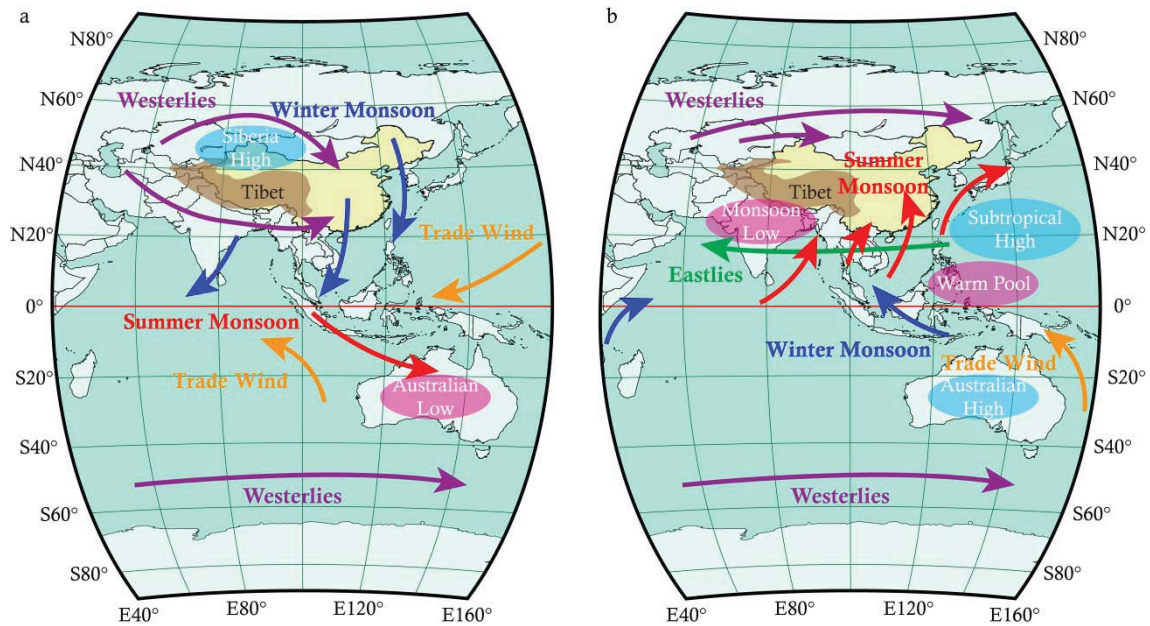
Fig. 1-2   Schematic view of the main atmosphere characteristics during the NH (A) winter and (B) summer. The thermal effect of lower boundary conditions changes seasonally, which causes seasonal reversal of the pressure system. This illustrates a pressure-driven exchange of monsoon circulation and migration of trade winds between Australia-East Asia territory. (modified from An, 2000)

1.2   Cave stalagmite $\delta^{18}O$ as AM proxy

1.2.1   Karstic system

In the karstic system, stalagmite is one kind of calcareous speleothems (cave precipitates), which can provide paleoclimatic records from closed-system caves with high humidity of ~100%. The dripwater with climatic/environmental information from outer environment permeates into soil and dissolves the carbon dioxide (CO_2), which

becoming carbonic acid (H_2CO_3). The carbonic acid dissolves the carbonate bedrock, becoming the solution which contains $Ca^{2+}_{(aq)}$ and $CO_3^{2-}{}_{(aq)}$. After the solution permeates into the carbonate cave, the calcareous speleothem ($CaCO_3$) precipitates by water evaporation or CO_2 degassing process (Fig. 1-3).

The advantages of stalagmite for paleoclamatic reconstruction are summarized in *Fairchild et al.*, 2006) as follows:

1. Some stalagmites can be precisely dated by radioisotope dating methods, such as U-Th dating, ^{14}C dating, and ^{210}Pb dating.

2. Stalagmites can grow continuously for 10^1 -10^5 years that can be used as the climatic proxies of different time scales.

3. The hiatus in a single stalagmite can probably be filled up by other stalagmites from the same cave.

4. Karstic caves are widely distributed that is beneficial for the comparison of regionally paleoclimatic study and the reproduction of climatic trend.

5. Due to the isolated system stalagmite is, after the precipitation, the climatic records which were preserved in the stalagmite are hardly varied by external factors and sequential internal processes.
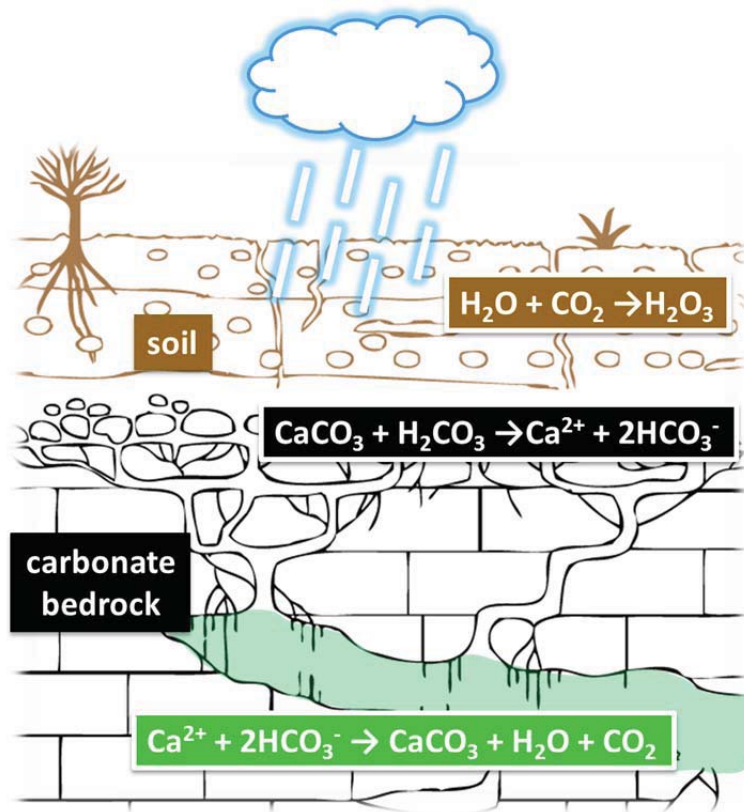
Fig. 1-3 Dissolutional and precipitative regimes of the karstic system (modified from Fairchild et al., 2006).

1.2.2 U-Th dating

U-Th dating, one of uranium-series dating methods, also called [230]Th dating (Faure, 1986; 1998), is commonly used for determining age of carbonate materials, such as speleothem and coral. This dating method is based on the decay principle of decay series, starting with [238]U and ending with stable [206]Pb by a series of α and β emissions, which contains [234]U and [230]Th as the longest-lived intermediate daughters. In [238]U decay series, the main radionuclides and their half-lives (M.Baum et al., 2002) are showed below.

Nuclides	^{238}U	$\longrightarrow$	^{234}U	$\longrightarrow$	^{230}Th	$----\rightarrow$	^{206}Pb
Half-life	4.47×10^9y		2.46×10^5y		7.54×10^4y		
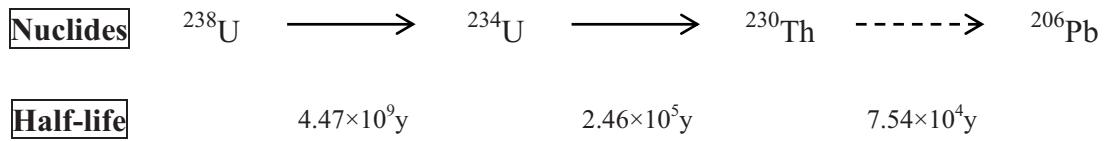
Under oxidizing conditions, uranium exists as U^{6+} and soluble in water mobile as $UO_2{}^{2+}$, whereas thorium exists as Th^{4+} and is insoluble in water. Therefore, deposited carbonate contains appreciable concentrations of U but is virtually free of Th. As a result, the activity of ^{230}Th in deposited carbonate is initially mostly equal to zero and increases as a function of time by decay of $^{234}U{}^{234}U$ and ^{238}U. Stalagmite is one kind of carbonate materials satisfies an important requirement for U-Th dating:

The ^{230}Th age equation is expressed as:

$$\left(\frac{^{230}Th}{^{238}U}\right)_{activity}=1+\left[\left(\frac{^{232}Th}{^{238}U}\right)\left(\frac{^{230}Th}{^{232}Th}\right)-1\right]e^{-\lambda_{230}t}+\frac{\delta^{234}U_{measured}}{1000}\left(\frac{\lambda_{230}}{\lambda_{230}-\lambda_{234}}\right)\times\left(1-e^{(\lambda_{234}-\lambda_{230})t}\right)$$

$$\lambda_{230}=\lambda_{230_{Th}}=9.1577\times10^{-6}yr^{-1} \qquad \lambda_{234}=\lambda_{234_U}=2.8263\times10^{-6}yr^{-1}$$

where t is age and λ is decay constant (Faure, 1986; Faure, 1998; Shen et al., 2008).

1.2.3 Oxygen isotope fractionation

The oxygen isotope variations of stalagmites can reflect the oxygen isotope variations of drip water from outer rainfall if stalagmite deposits at an oxygen isotopic equilibrium condition (Dansgaard, 1964). During the of stalagmite precipitation, four major fractionation factors affect the carbonate oxygen isotope ratio, including latitude (distance) effect, altitude effect (~1.5-3.5‰/km) (Gonfiantini et al., 2001), amount

(rainfall) effect (about -0.02‰/mm in tropical region) (Rozanski et al., 1993; Gonfiantini et al., 2001), and temperature effect (-0.20‰ ~ -0.25‰/℃) (O'Neil et al., 1969; Kim and O'Neil, 1997).

Fig. 1-4   (Left) Latitude (distance) effect. (Right) Altitude effect.
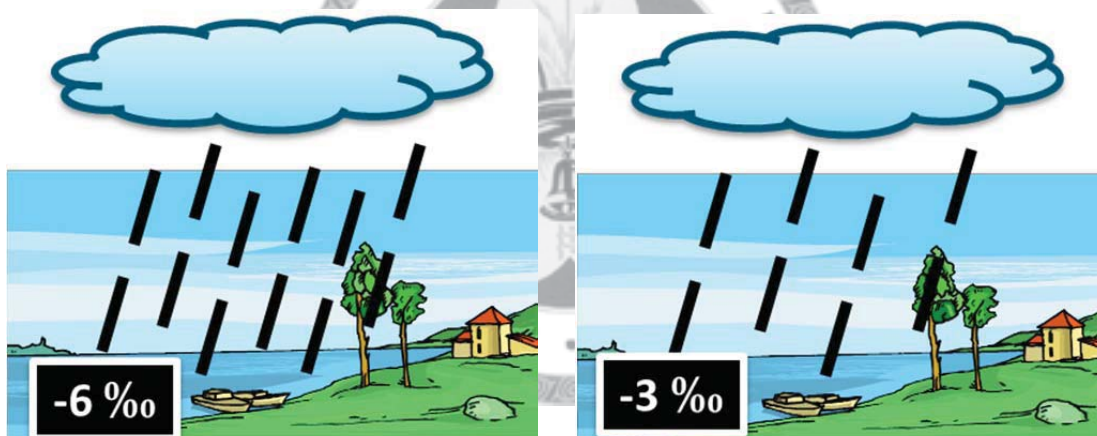
Fig. 1-5   Rainfall effect. (left/right) The $\delta^{18}O$ value of rainfall is low/high when the intensity of rainfall is strong/weak.
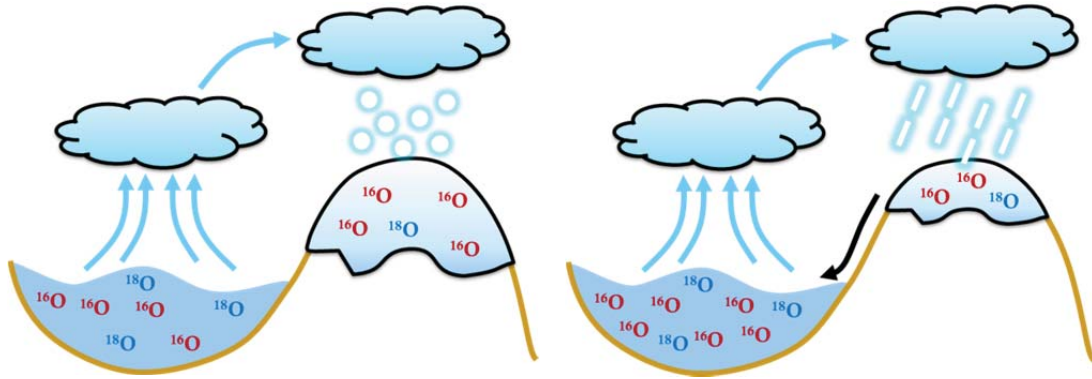
Fig. 1-6   Temperature effect. (left/right) During the glacial/interglacial period, the $\delta^{18}O$

value of sea water become high/low.

1.2.4   Stalagmite oxygen isotope proxy for AM

The oxygen isotope values of stalagmites as the proxies for paleoclimatic reconstruction had been developed over decades (Wang et al., 2001; Dykoski et al., 2005; Kelly et al., 2006; Wang et al., 2006; Wang et al., 2008; Cheng et al., 2009; Zhao et al., 2010; Cheng et al., 2012), and the proxies represent different significances at different regions.

At low-to-mid latitude AM areas, even the seasonal changes of air temperature out of cave over ±15℃, the cave temperature in deep channel can hold constant with a seasonal change of less than 0.5℃ and represent annual mean temperature out of cave (e.g., Li et al., 2011). Therefore, the observed variations of stalagmite $\delta^{18}O$ values are over ±6‰, which cannot be explained by temperature change.

The stalagmite $\delta^{18}O$ variations should mainly be controlled by the rainfall 18O if carbonate deposits at an oxygen isotopic equilibrium condition in cave. Previous studies (Wang et al., 2008; Cheng et al., 2009; Zhao et al., 2010; Cheng et al., 2012) had

indicated that stalagmite $\delta^{18}O$ record in AM regions represent as summer precipitation intensity, in repose of ASM intensity. High stalagmite $\delta^{18}O$ values suggest a weak ASM and also a dry condition; low $\delta^{18}O$ values represent a dry condition and strong ASM period.

1.2.5 Hendy Test

The oxygen isotope values of stalagmites can represent as climatic/environmental proxies only if carbonate precipitates at an isotopic equilibrium condition. Under a strong kinetic fractionation during stalagmite precipitation, oxygen isotopic value will be biased and cannot reflect original climatic/environmental signal. Hendy test (Hendy, 1971) is a method for testing whether the stable isotope value of carbonate is at an equilibrium condition or not and can help exclude unsuitable stalagmites for paleoclimatic reconstruction. Two scenarios are used. (1) Along a single layer, the $\delta^{18}O$ values of the coeval subsamples should be nearly constant and (2) not correlated with $\delta^{13}C$ values and the distances to the center of growth axis.

1.3 Previous studies and debates

Recent studies have led to significant advances in understanding of AM evolution on different time scales in Quaternary (e.g., An, 2000; Wang et al., 2001; 2008; Fleitmann et al., 2003; 2004; Cheng et al., 2006; 2009; Zhang et al., 2008; An et al., 2011). Cave stalagmites have advantages of absolute and high-precision chronology and abundant proxies (e.g., Fairchild et al., 2006). Up-to-date, AM variation over past 380

kyr BP has been reconstructed using Chinese stalagmite oxygen isotope records (Fig. 1-7) (Wang et al., 2001; 2008; Cheng et al., 2006; Kelly et al., 2006; Cheng et al., 2009; 2012). However, those 100s-kyr records were mainly from only one cave, called Sanbao (31°40'N, 110°26'E), located in Hubei Province, China (Wang et al., 2008). This brings tremendous uncertainties in interpreting long-term AM records. Moreover, interpreting monsoon proxy records of centennial-to-orbital scales are complicated by changing sources of monsoon winds and/or precipitations, and the interactions with tropical storminess, cold surges from the north or west, and equatorial Pacific circulation changes from the east.
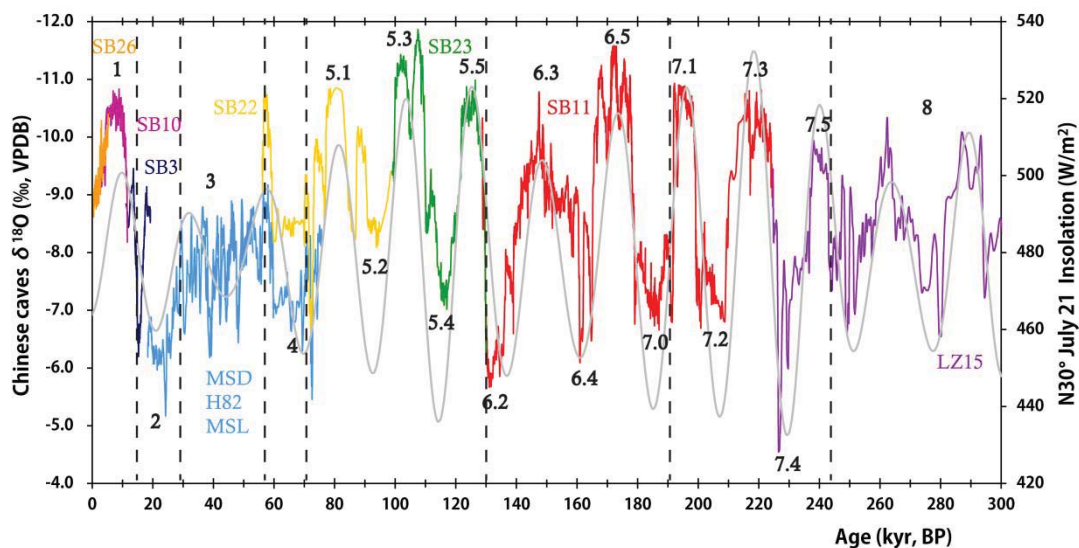
Fig. 1-7   The stalagmite $\delta^{18}O$-inferred AM evolution at 0-300 kyr BP from the

previous Chinese caves, including Sanbao cave (stalagmites SB26, SB10,

SB3, SB22, SB23, and SB11) (Wang et al., 2008), Hulu cave (stalagmites

MSD, H82, and MSL) (Cheng et al., 2006), and Linzhu cave (stalagmite

LZ15) (Cheng et al., 2009). The gray line is the NH summer insolation (NHSI)

on 21 July at 30˚N. Vertical dashed lines are the MIS boundaries.

During the marine isotope stage (MIS) 6, Sanbao records show prevailing strong ASM events at MIS6.3 (139-160 ka) and MIS 6.5 (165-178 ka) while the a glacial time at 130-191 ka (Fig. 1-8c) (Wang et al., 2008); however, loess geomagnetic evidence suggests a long-term weak ASM condition which primarily follows the glacial/interglacial periods. (Fig. 1-8a & b) (Sun et al., 2006).
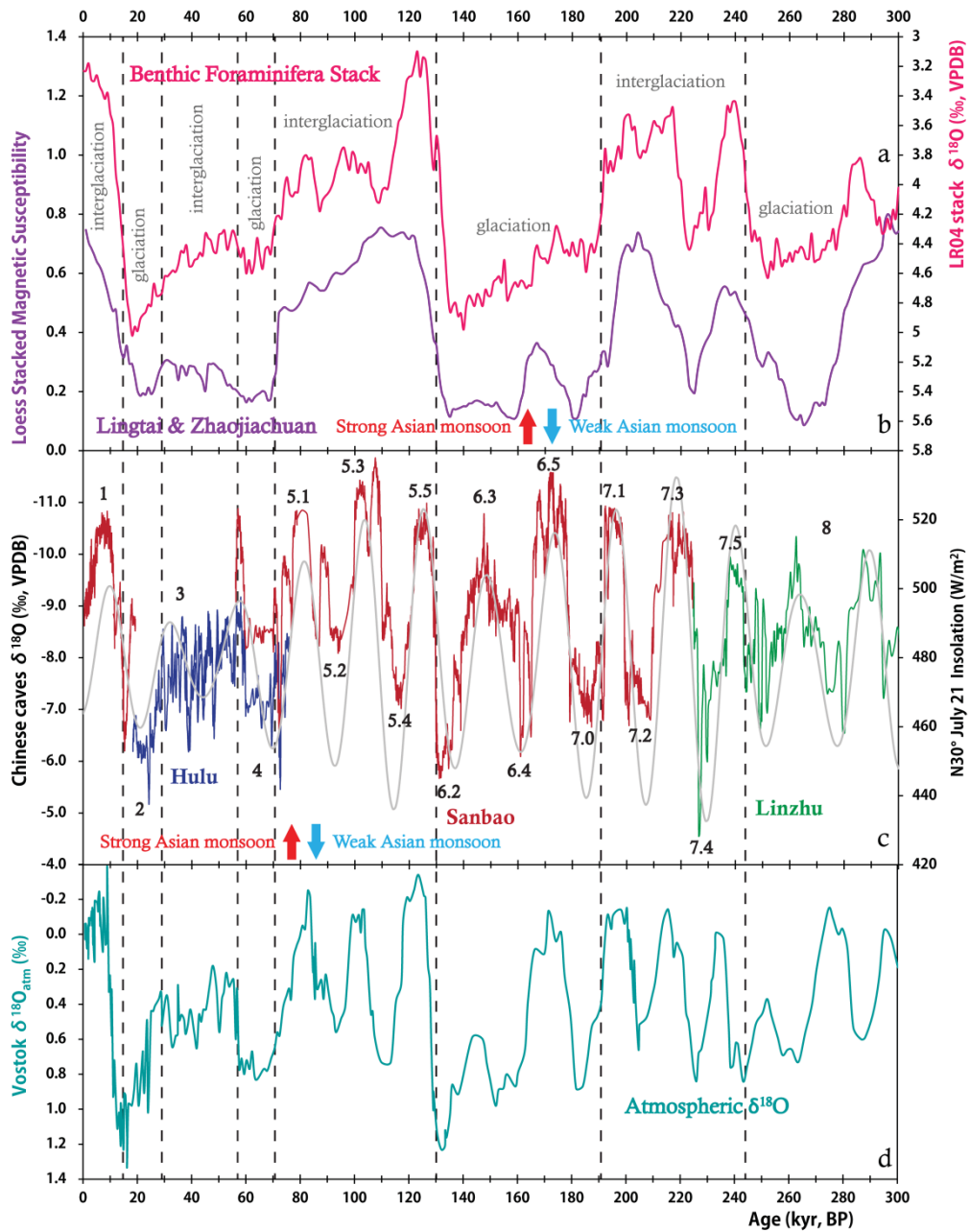
Fig. 1-8   (a) LR04 Benthic Stack $\delta^{18}O$ record, reflecting global ice volume (Lisiecki and Raymo, 2005). (b) Loess magnetic susceptibility records of Lingtai and Zhaojiachuan (Sun et al., 2006). (c) $\delta^{18}O$ records of previous Chinese stalagmites (Cheng et al., 2006; 2009; Wang et al., 2008). Gray curve is the NHSI on 21 July at 30˚N. (d) Atmospheric $\delta^{18}O$ variation from Vostok ice core, Antarctica (Sowers et al., 1991; Petit et al., 1999).

Sanbao records show prevailing strong ASM events at MIS 6.3 (139-160 kyr BP) and MIS 6.5 (165-178 kyr BP) during a glacial time at 130-191 kyr BP (Fig. 1-8c) (Wang et al., 2008). However, loess geomagnetic evidence suggests a long-term weak ASM condition which primarily follows the glacial/interglacial periods. (Fig. 1-8a & b) (Sun et al., 2006). Sanbao records show the extraordinarily weakest summer monsoon at the penultimate deglaciation (MIS 6.2; 128-136 kyr BP) and the strongest one at the glacial time (MIS 6.5; 166-177 kyr BP). To clarify that the weakest ASM intensities during the penultimate deglaciation in Hubei province and the strong ASM events at the glacial time are site-specific or dominant in the entire East Asia, we collected stalagmite samples with deposition time intervals from Yangkou Cave (Chongqing; 29°2'N, 107°12'E; altitude: 2140 m) located 400 km southwest to Sanbao Cave (Fig. 2-1). Three major topics addressed in this study are: (1) To verify that AM events during 134-200 ka inferred from Sanbao cave are site-specific or dominant in the entire mainland. (2) To clarify the different AM implications between stalagmite and loess. (3) To evaluate different climatic/environmental factors on stalagmite $\delta^{18}O$ record in AM region.

Chapter 2   Regional settings and Methods

2.1   Studied site and research material

2.1.1   Location of Yangkou cave

Stalagmites were collected from Yangkou cave (29°2'N, 107°12'E; altitude: 2140 m), located at Mount Jinfo National Park, Chongqing City, China (Fig. 2-1). Yankou cave is a limestone cave about 400 km southwest to Sanbao cave (Hubei province; 31°40'N, 110°26'E) (Wang et al., 2008).
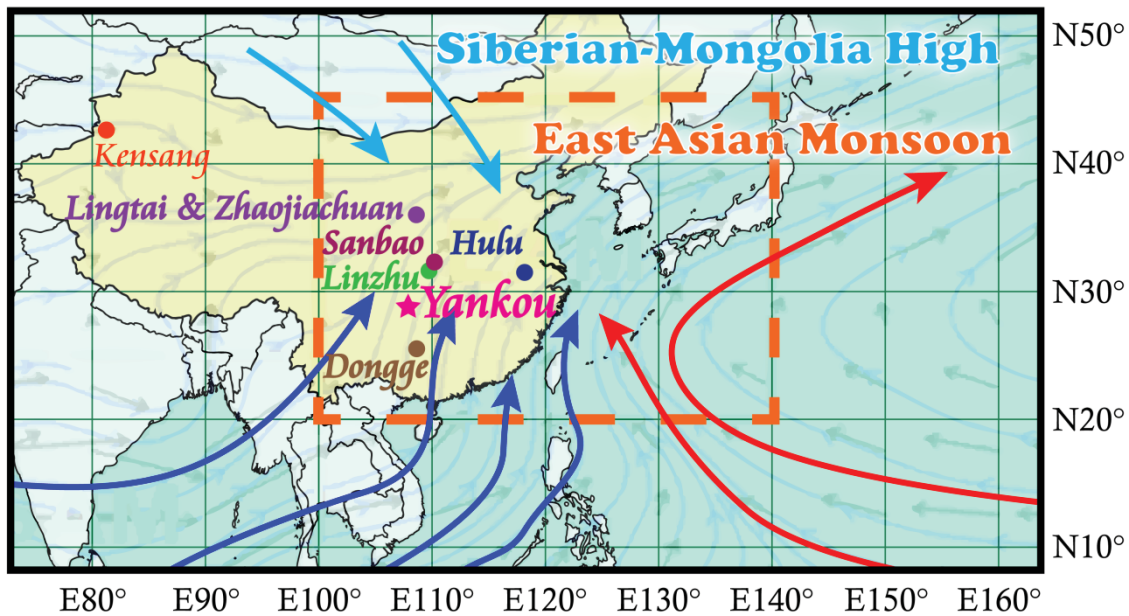
Fig. 2-1   Locations of Chinese caves, including Yangkou (this study), Sanbao (Wang et al., 2008), Linzhu (Cheng et al., 2009), Hulu (Cheng et al., 2006), Dongge (Kelly et al., 2006), and Kensang (Cheng et al., 2012) and Loess sites, Lingtai and Zhaojiachuan (Sun et al., 2006).

2.1.2 Regional settings

The mean annual temperature in Yangkou cave is very stable at 16.5℃. The regional climate is dominated by AM. The annual rainfall is 1400-1500 mm and concentrates in summer. The winter (December-February) rainfall is only about 8%.
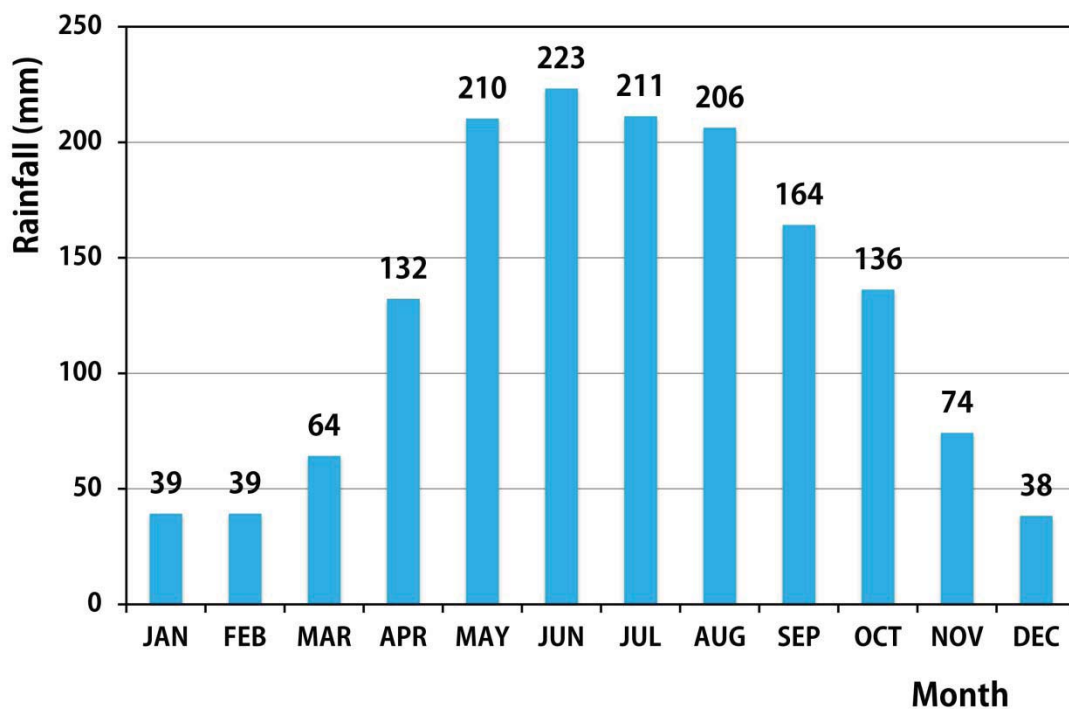
Fig. 2-2 Long-term averaged monthly rainfall record of Mt. Jinfo during 1954-1994 (SINA, 2010).

2.1.3 Field work and sample collection

Two field trips to Yangkou cave were conducted on 2010/10/16 and 2011/07/19, respectively. Thirty two stalagmites were collected. Additional 14 stalagmites from the same cave were provided by Dr. Ting-Yong Li and Dr. Xun-Lin Yang of the Southwest University, Chongqing City, China. Deposition intervals of all 46 stalagmites were

screened with U-Th dating methods. Five stalagmites with time spans of interest were selected for this study.

2.2 Experiment

2.2.1 Subsampling

Stalagmite samples were halved and polished (Fig. 2-3). For U-Th dating, powdered subsample, 60-80 mg each, was drilled. For Hendy Test (Hendy, 1971), 6-8 powdered coeval subsamples, 60-120 μg each, were drilled. To obtain oxygen time series, 60-120 μg subsamples were drilled at a 0.5-3.0 mm intervals along the growth axis (Fig. 2-4). Some subsamples were drilled bulk pieces. They were crushed gently into tiny fragments, which were kept in a cleaned glass vial. They were ultrasonicated with pure H_2O 3 times to get rid of any contamination and then dried.

In this study, along the growth axes, total 612 subsamples were collected from five stalagmites, YK05, YK12, YK23, YK47, and YK61, for serial oxygen isotope measurement.

Fig. 2-3 (a) The stalagmite was being halved. (b) An example of halved stalagmites. (c)

A polished stalagmite from Yangkou cave.
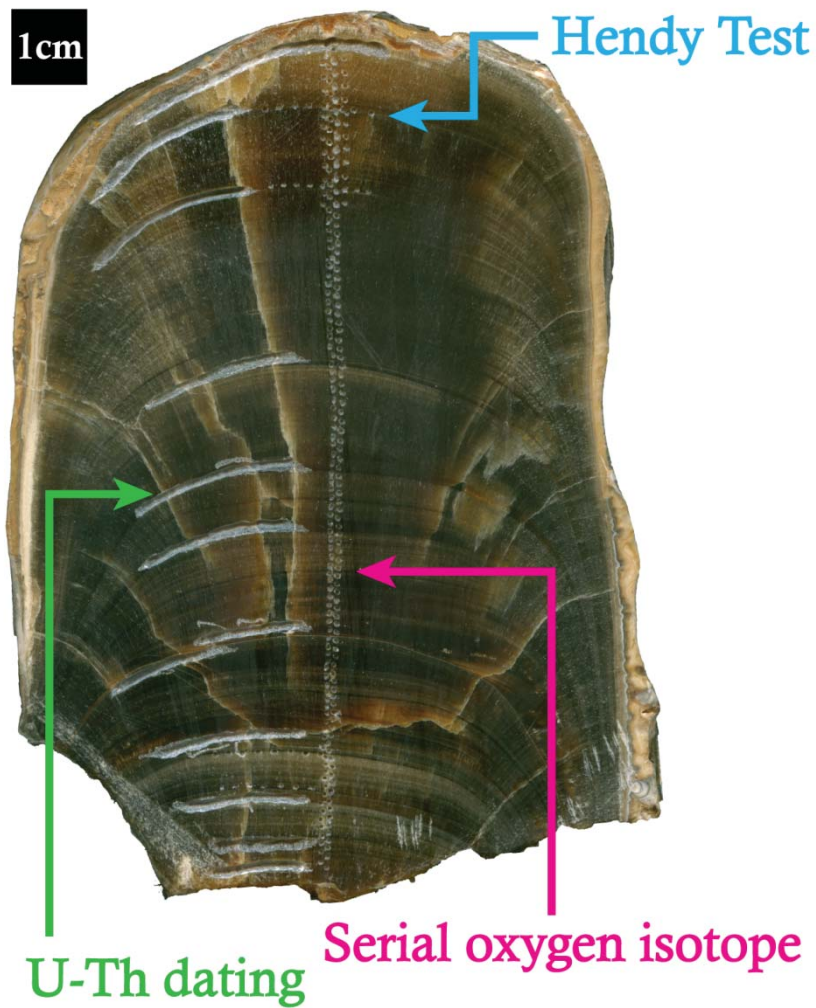
Fig. 2-4   Stalagmite ID here with subsamples for oxygen isotope measurement (pink), U-Th dating (green), and Hendy Test (crayon).

2.2.2 Labware

Labware used in this study includes Teflon beaker, bottle, and column, PE/PP bottle, centrifuge tube, vial, pipette tip, and porous PP column frit. For reducing chemical blanks, all labware was acid-cleaned prior to U-Th chemistry (Shen et al., 2003). Detailed cleaning procedure is available in Appendix I. Milli-Q Element water (18.2 Ω) and ultrapure acids, including HNO_3 (Seastar), HCl (Seastar), and $HClO_4$

(Merck), were used for chemistry.

2.2.3 Chemical procedure for stalagmite U-Th dating

To reduce the contamination, the chemical procedure for U-Th dating was performed in the class-10,000 clean room with independent class-100 benches and hoods.

Sample digestion

1. Powdered or bulk subsample was weighted and kept in a 30-ml Teflon beaker.

2. Sample was covered with pure water and dissolved gradually by adding drops of $14 N$ HNO_3.

3. Appropriate amount of ^{229}Th-^{233}U-^{236}U spike solution was added into the sample solution and weighted.

4. Ten drops of $HClO_4$ was added into the sample solution to get rid of the organic matter.

5. One drop of $FeCl_2$ solution was added for iron co-precipitation.

6. With the Teflon beaker closed, the sample solution was reflux at $200°C$ on a hotplate over 12 hours to earn U-Th isotopic equilibrium and decompose organic molecular completely.

7. Sample solution was dried on a hotplate at $250°C$.

Iron co-precipitation & centrifugation

1. Dried sample was covered with ~1-2 ml H_2O , re-dissolved with ~1-2 ml 2 N
    HCl, and then transferred into a PE centrifuge tube.

2. Appropriate amount of NH_4OH was dropwisely added into the sample solution
    till $Fe(OH)_3$ precipitation (for uranium and thorium co-precipitated)..

3. Separated by centrifugation, the suspension was discarded and the residue was
    rinsed with H_2O. Repeat this step 3 times.

4. Ten drops of 14 N HNO_3 was added to re-dissolve the residue, and the sample
    solution was transferred back into the original and cleaned Teflon beaker.

5. The sample solution was added with 2 drops of $HClO_4$ and dried on a hotplate at
    250℃.

6. The dried sample was re-dissolved with 1 drop of 14 N HNO_3 and then dried at
    250℃. This step was repeated for 3 times to keep cations in nitric form.

7. An amount of 0.5 ml 7 N HNO_3 was added to re-dissolve the dried sample for ion
    exchange column separation.

Extract uranium and thorium by ion exchange column

1. Containing AG 1-X8 resin, an anion-exchange column, about 6-7 cm in length,
    was prepared.

2. The column was preconditioned with 1 column volume (cv) of H_2O (with 1 drop of 14N HNO_3), 1 drop of 7 N HNO_3, and then 1 cv of 7 N HNO_3.

3. The prepared sample solution was loaded onto the preconditioned column.

4. One drop of 7 N HNO_3 and 1 cv of 7 N HNO_3 were added sequentially to elute Fe^{3+}.

5. During the previous step, the 30-ml Teflon breaker was refluxed for ~10 min with 15 ml 1% Aqua Regia (with 0.005 N HF) and rinsed by H_2O to decompose possible organic material.

6. One drop of 6 N HCl, 1/3 cv of 6 N HCl, and then 1 cv of 6 N HCl were added to column to collect thorium fraction in the cleaned original 30-ml Teflon beaker. Two drops of $HClO_4$ was added into the beaker for decomposition of organic matter.

7. One drop of H_2O and 1 cv of H_2O were added into column to collect uranium fraction in a cleaned 10-ml Teflon breaker. Two drops of $HClO_4$ was added into the sample solution for decomposition of organic matter.

8. Both extracted uranium and thorium fractions were dried on a hotplate at 250℃.

9. The dried samples were re-dissolved with 1 drop of $HClO_4$ for getting rid of the organic matter and dried on the hotplate at 250℃.

10. The dried samples were re-dissolved with 1 drop of 14 N HNO_3 and then dried at 250℃ three times.

11. The extracted uranium and thorium samples were re-dissolved with 0.5 ml of 1% HNO_3 (+0.005 N HF) and transferred to PE vial for instrumental analysis.

2.3 Instrumentation

2.3.1 U-Th dating instrumentation

A high resolution multi-collector inductively coupled plasma mass spectrometer (MC-ICP-MS) with secondary electron multiplier (SEM) protocols, Thermo-Fisher, Neptune, was used for U-Th dating (Fig. 2-5). U-Th dating techniques and chemical procedure were developed in the HISPEC, Department of Geosciences, National Taiwan University (Shen et al., 2012). The instrumental sensitivities are 2-4%, with a precision of $\pm$1-2‰ (2σ) for abundance determinations of 50-200 fg ^{234}U (1-4 ng ^{238}U) or ^{230}Th. One international standard, New Brunswick Laboratories Certified Reference Material 112A (NBL-112A) was used for calibrating biases (Shen et al., 2012).

Fig. 2-5   MC-ICP-MS with SEM protocols, Thermo-Fisher, Neptune, used for U-Th

isotopic measurement.

2.3.2   Oxygen isotope measurement

Micromass IsoPrime Isotope Ratio Mass Spectrometer (IsoPrime IRMS) (Fig. 2-6)

was used for the oxygen and carbon isotope analyses with 1-sigma precision of $\pm 0.03‰$

and $\pm 0.05‰$, respectively

The measurement was performed in three laboratories, including Stable Isotope

Laboratory, Department of Earth Sciences, National Taiwan Normal University,

Peleo-Environment, Geochemistry and Stable Isotope Laboratory, School of

Geographical sciences, Southwestern Normal University, and NeoTectonics Laboratory,

Department of Geosciences, NTU.

Fig. 2-6　Micromass IsoPrime IRMS used for the oxygen and carbon isotope analyses.

Chapter 3　Results

3.1　U-Th dating data

After screening, five stalagmites, YK05, YK12, YK23, YK47, and YK61, were selected. The lowest uranium concentration of the subsamples is 0.24 ppm (YK47-10), whereas the highest one is 13 ppm (YK12-5). Age (before AD 1950) intervals are 179.6-187.8 kyr (YK05), 133.4-181.9 kyr (YK12), 172.6-206.8 kyr (YK23), 74.9-132.1 kyr (YK47), and 95.4-173.5 kyr (YK61), respectively (Table 3-1 to 3-5 and Fig. 3-2 to 3-6). The detailed U-Th isotopic and concentration data and dates are available in Appendix II.

The average growth rates are 4.3 yr/mm (YK05), 42.5 yr/mm (YK12), 38.6 yr/mm (YK23), 41.0 yr/mm (YK47), and 41.5 yr/mm (YK61), respectively. However, except YK05, some hiatus exist in the other stalagmites that sometimes the actual growth rates change largely even in the same stalagmite sample (Fig. 3-1).

Table 3-1 Five selected stalagmites, YK05, YK12, YK23, YK47 and YK61

Sample ID	Length (cm)	Age (kyr BP)	Descriptions
YK05	19.15	179.64-187.83	Continuously growth, no hiatus. Dating points: 10
YK12	11.40	133.44-154.18 166.42-181.87	One hiatus. Dating points: 11
YK23	8.85	172.62-177.52 186.96-188.72 193.22-198.97 200.83-206.84	Three hiatus. Dating points: 11
YK47	13.95	74.87-79.04 84.92-102.54 108.01-110.15 129.99-132.14	Only the part 9.7-13.95 cm dated. Three hiatus. Dating points: 8
YK61	18.80	95.44-103.85 123.50-131.44 139.62-173.51	Two hiatus. Dating points: 18
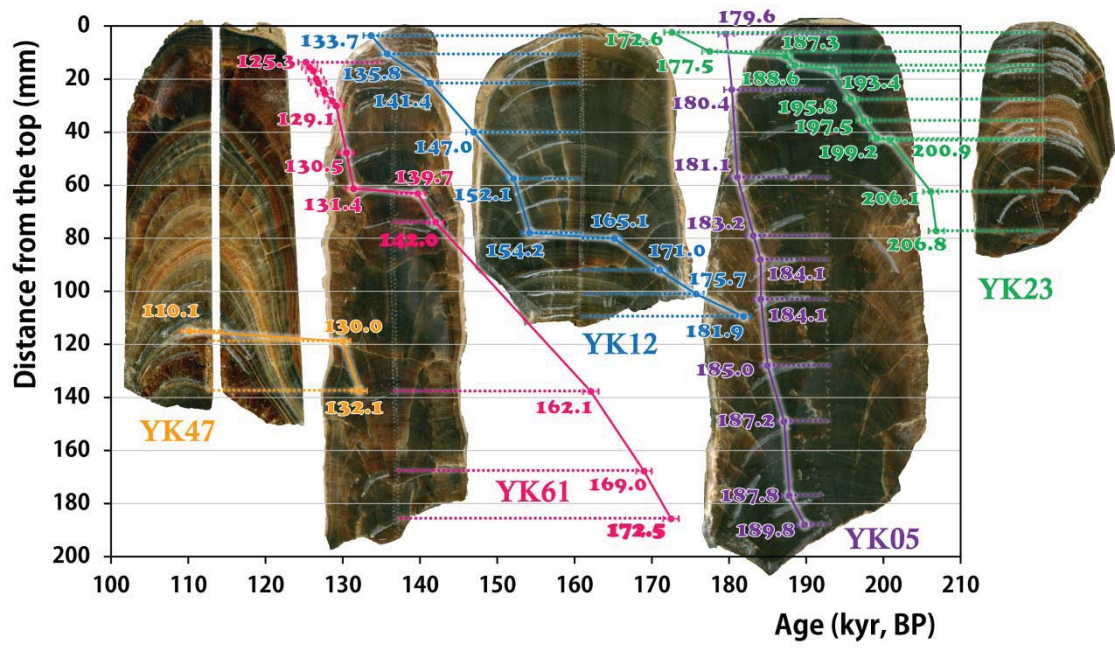
Fig. 3-1 The growth rate of five stalegmites selected from Yangkou cave.

Table 3-2   Subsample ^{230}Th dates of stalagmite YK05.

Subsample ID	Depth (mm)	Age (kyr BP)	2σ Error (kyr)
YK05-01	3.0	179.6	±1.3
YK05-02	24.0	180.4	±1.6
YK05-05	57.0	181.1	±1.4
YK05-07	79.0	183.2	±1.7
YK05-08	88.0	184.1	±1.6
YK05-09	103.0	184.1	±1.5
YK05-10	128.0	185.0	±1.4
YK05-13	149.0	187.2	±1.8
YK05-14	177.0	187.8	±1.1

179,643 ± 1325

180,375 ± 1600

181,102 ± 1438

183,171 ± 1713

184,103 ± 1611

184,143 ± 1499

184,999 ± 1436

187,159 ± 1841

187,826 ± 1128

189,815 ± 1694

YK05
^{230}*Th dates (kyr, BP)*
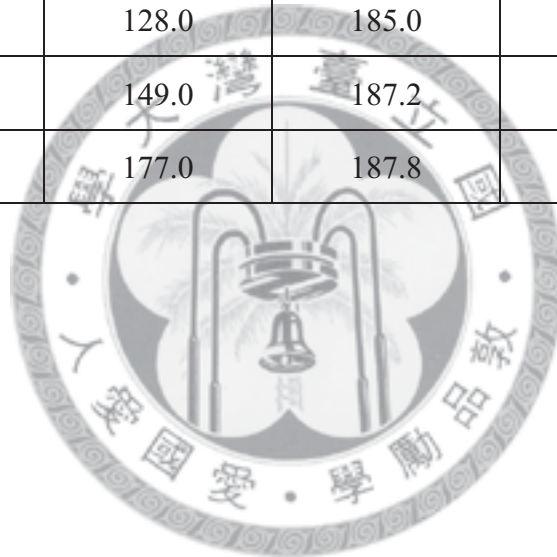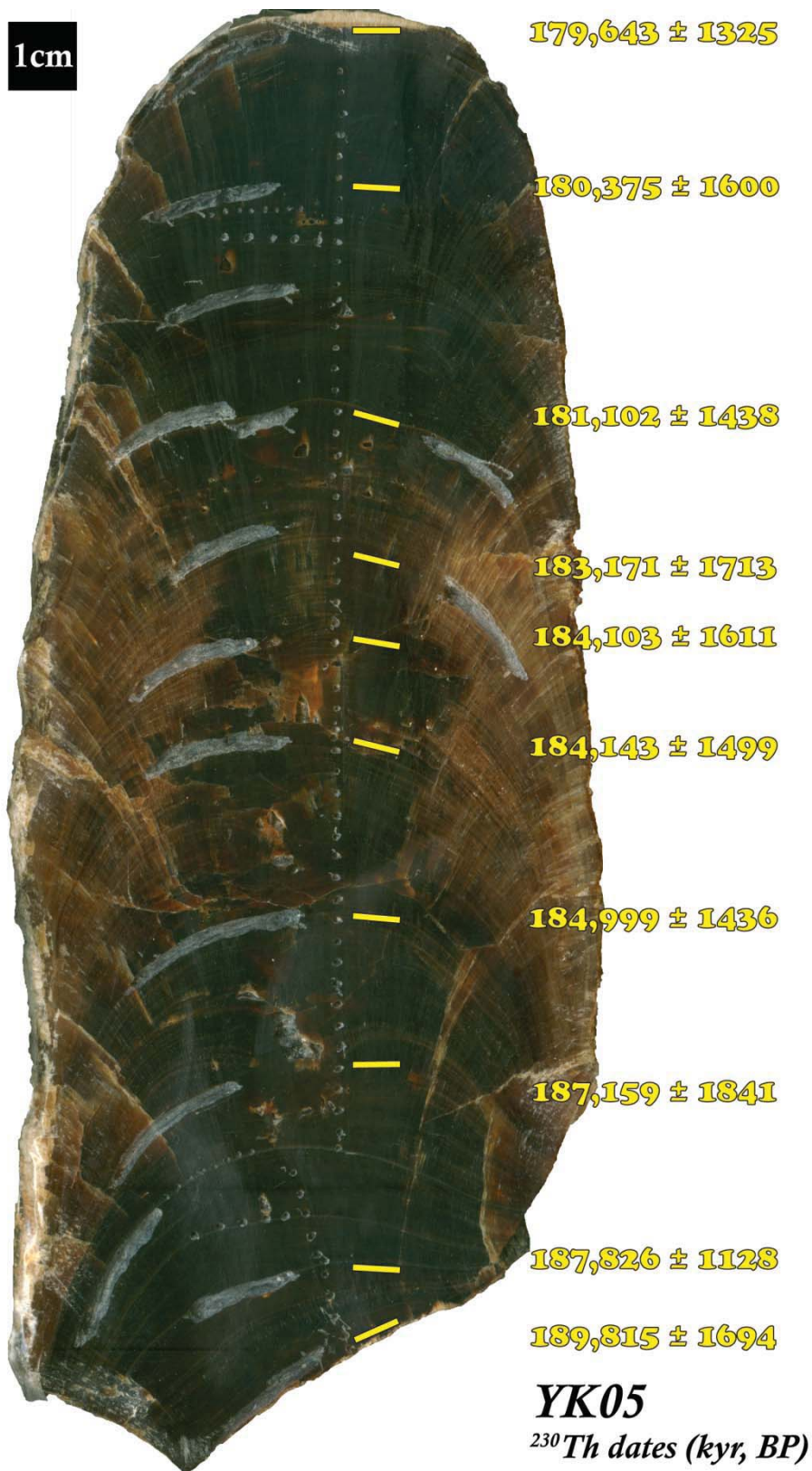
Fig. 3-2　Stalagmite YK05. The solid lines are the ^{230}Th dating points.

Table 3-3   Subsample ^{230}Th dates of stalagmite YK12.

Subsample ID	Depth (mm)	Age (kyr BP)	Error (kyr, 2σ)
YK12-01	3.6	133.7	±0.5
YK12-02	10.5	135.8	±0.6
YK12-03	21.5	141.4	±0.5
YK12-04	40.0	147.0	±0.7
YK12-05	57.5	152.1	±0.6
YK12-07	78.0	154.2	±0.5
YK12-08	80.0	165.1	±0.5
YK12-09	92.0	171.0	±1.2
YK12-10	101.0	175.7	±0.6
YK12-11	109.5	181.9	±0.7

133,690 ± 462

135,777 ± 511

141.362 ± 463

146.978 ± 670

152,138 ± 622

hiatus 154,235 ± 485

165,120 ± 1071

170,993 ± 643

175,725 ± 717

181,866 ± 770

YK12
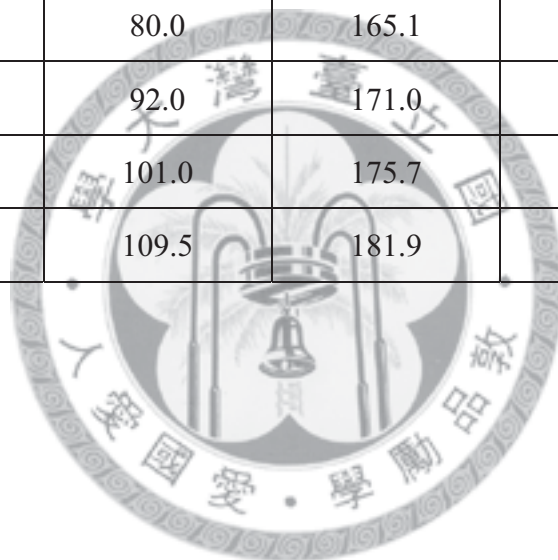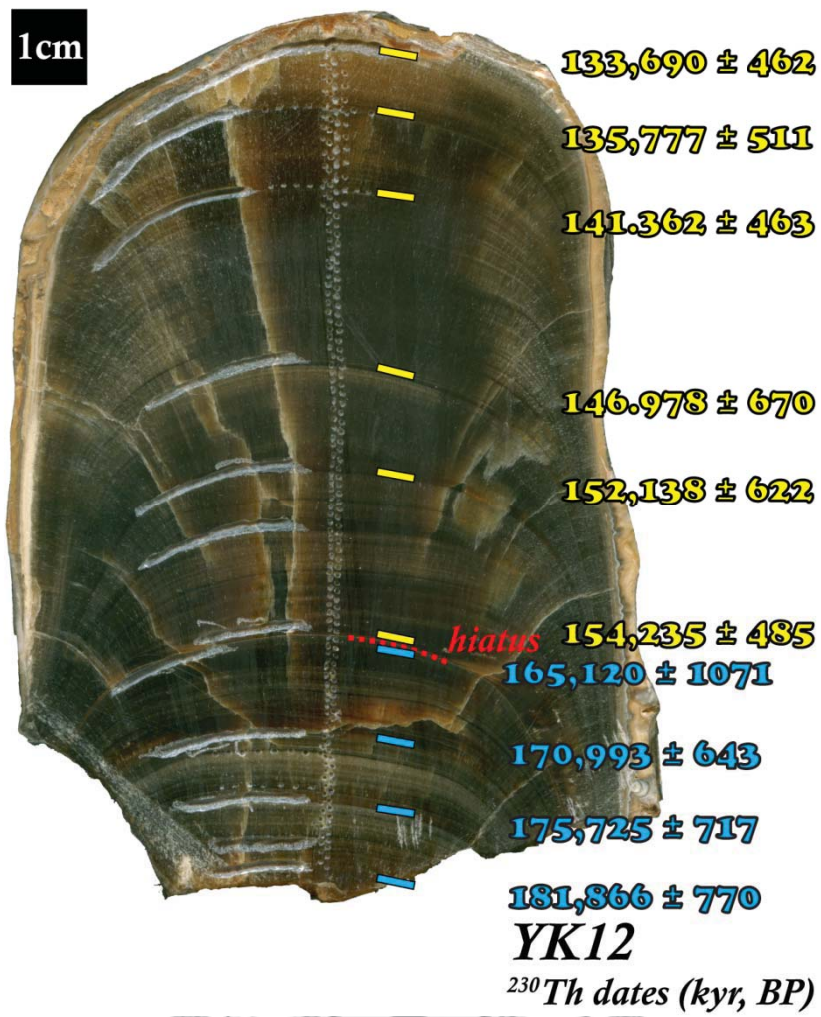
^{230}*Th dates (kyr, BP)*

Fig. 3-3   Stalagmite YK12. The solid lines are the ^{230}Th dating points and the dash

line is the precipitated hiatus.

Table 3-4   Subsample ^{230}Th dates of stalagmite YK23.

Subsample ID	Depth (mm)	Age (kyr BP)	Error (kyr, 2σ)
YK23-02	2.4	172.6	±1.0
YK23-03	9.6	177.5	±0.9
YK23-04	11.2	187.3	±1.0
YK23-05	14.8	188.6	±1.0
YK23-06	16.8	193.4	±1.0
YK23-07	27.6	195.8	±0.9
YK23-08	35.6	197.5	±1.1
YK23-10	42.4	199.2	±11
YK23-11	43.0	200.9	±1.1
YK23-13	62.4	206.1	±1.2
YK23-14	77.2	206.8	±1.3
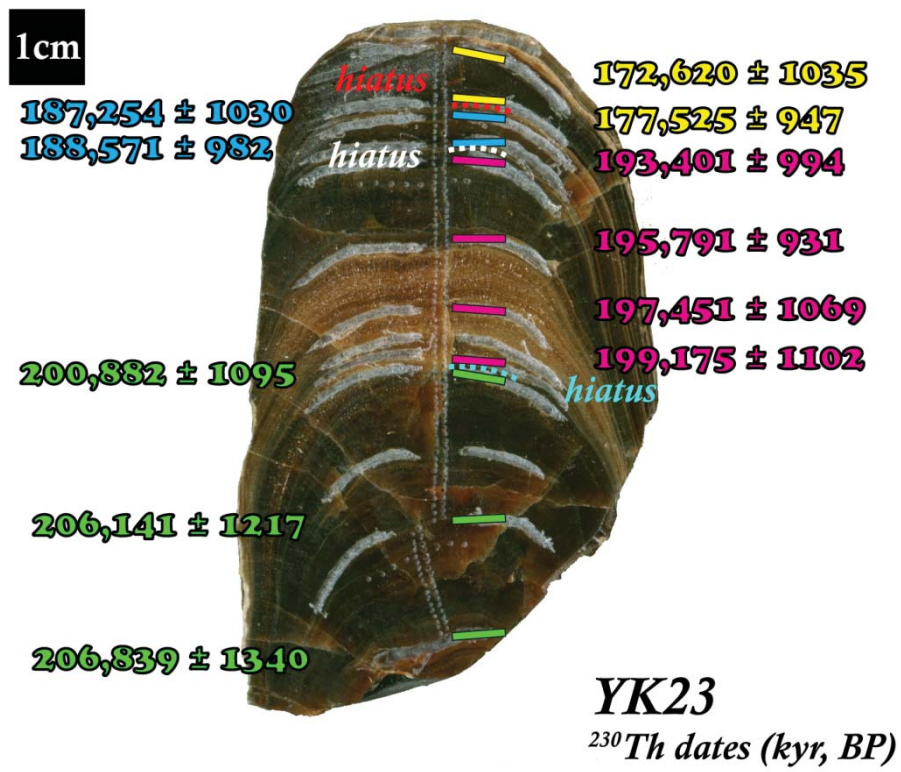
Fig. 3-4 Stalagmite YK23. The solid lines are the ^{230}Th dating points and the dash lines are the precipitated hiatus.
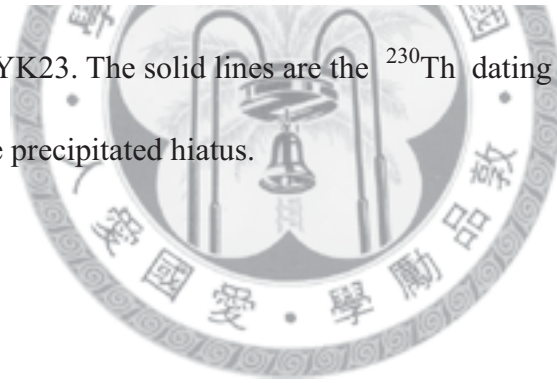
Table 3-5 Subsample ^{230}Th dates of stalagmite YK47.

Subsample ID	Depth (mm)	Age (kyr BP)	Error (kyr, 2σ)
YK47-10	97.2	74.9	±0.6
YK47-09	105.5	79.0	±1.1
YK47-08	107.5	84.9	±0.6
YK47-07	109.9	102.5	±1.9
YK47-06	112.2	108.0	±1.4
YK47-05	115.0	110.1	±1.4
YK47-03	118.8	130.0	±0.9
YK47-01	137.5	132.1	±0.4

1cm

74,870 ± 384

hiatus

79,044 ± 556

84,915 ± 927

108,009 ± 1398

102,535 ± 1039

110,148 ± 1363

hiatus

129,991 ± 612

hiatus

132,144 ± 566

YK47
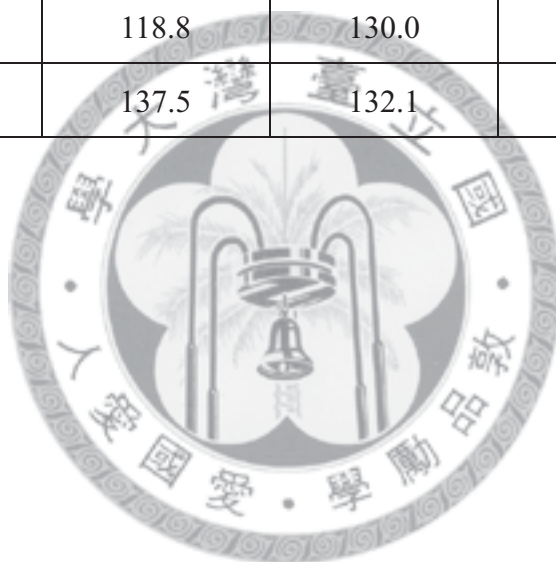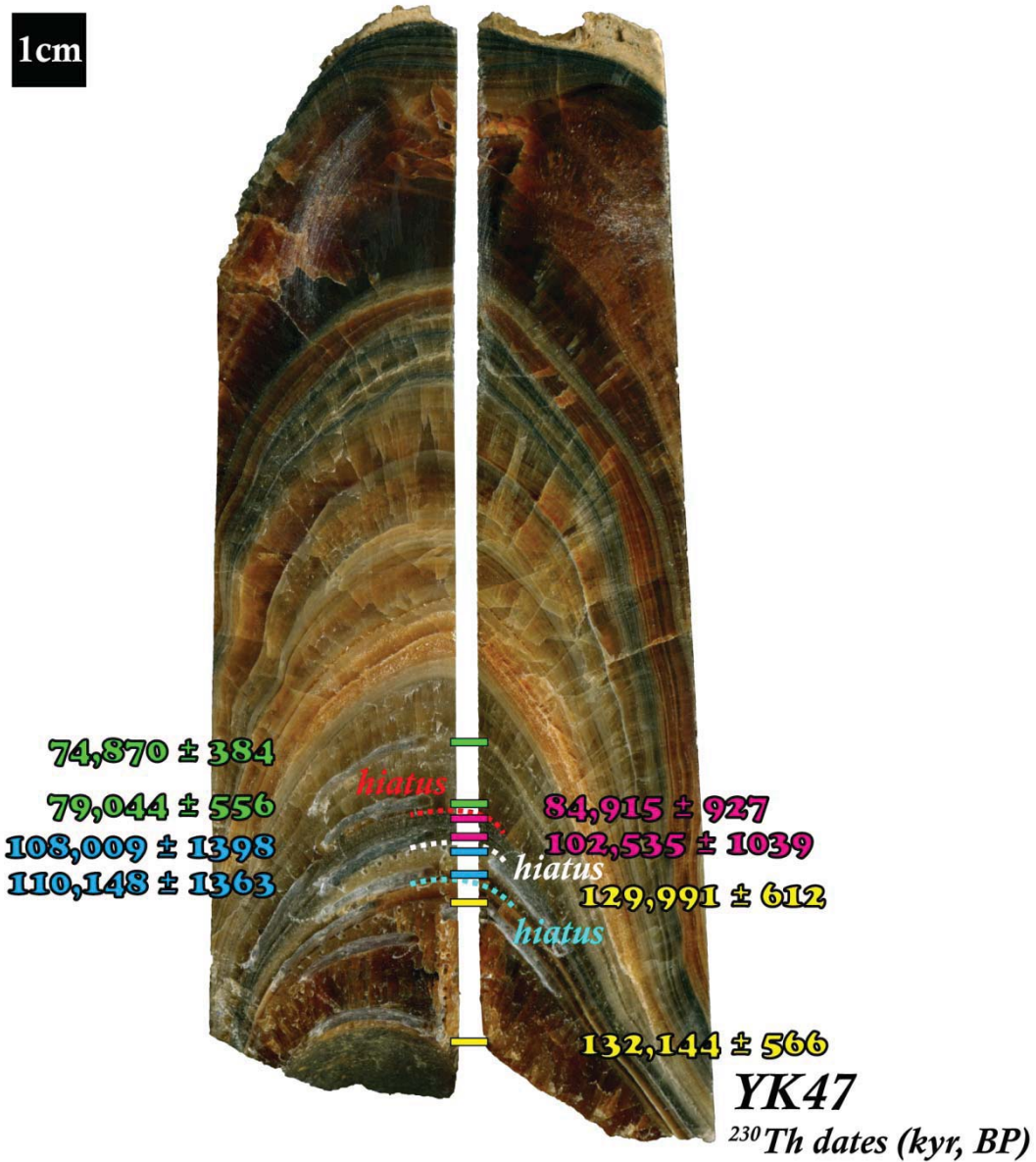
^{230}Th *dates (kyr, BP)*

Fig. 3-5   Stalagmite YK47. The solid lines are the ^{230}Th dating points and the dash

lines are the precipitated hiatus.

Table 3-6　Subsample ^{230}Th dates of stalagmite YK61.

Subsample ID	Depth (mm)	Age (kyr BP)	Error (kyr, 2σ)
YK61-01	1.6	97.2	±0.2
YK61-02	5.4	103.2	±0.4
YK61-04	13.6	125.3	±0.5
YK61-05	15.5	125.7	±0.4
YK61-06	17.0	126.2	±0.4
YK61-07	20.0	126.6	±0.5
YK61-08	21.5	126.9	±0.6
YK61-09	24.1	127.5	±0.7
YK61-10	25.6	127.7	±0.6
YK61-11	28.3	128.6	±0.5
YK61-12	30.1	129.1	±0.4
YK61-13	47.8	130.5	±0.5
YK61-14	61.3	131.4	±0.5
YK61-15	63.1	139.7	±0.4
YK61-16	74.0	142.0	±0.6
YK61-18	137.8	162.1	±0.9
YK61-19	167.8	169.0	±0.8
YK61-20	185.8	172.5	±0.8
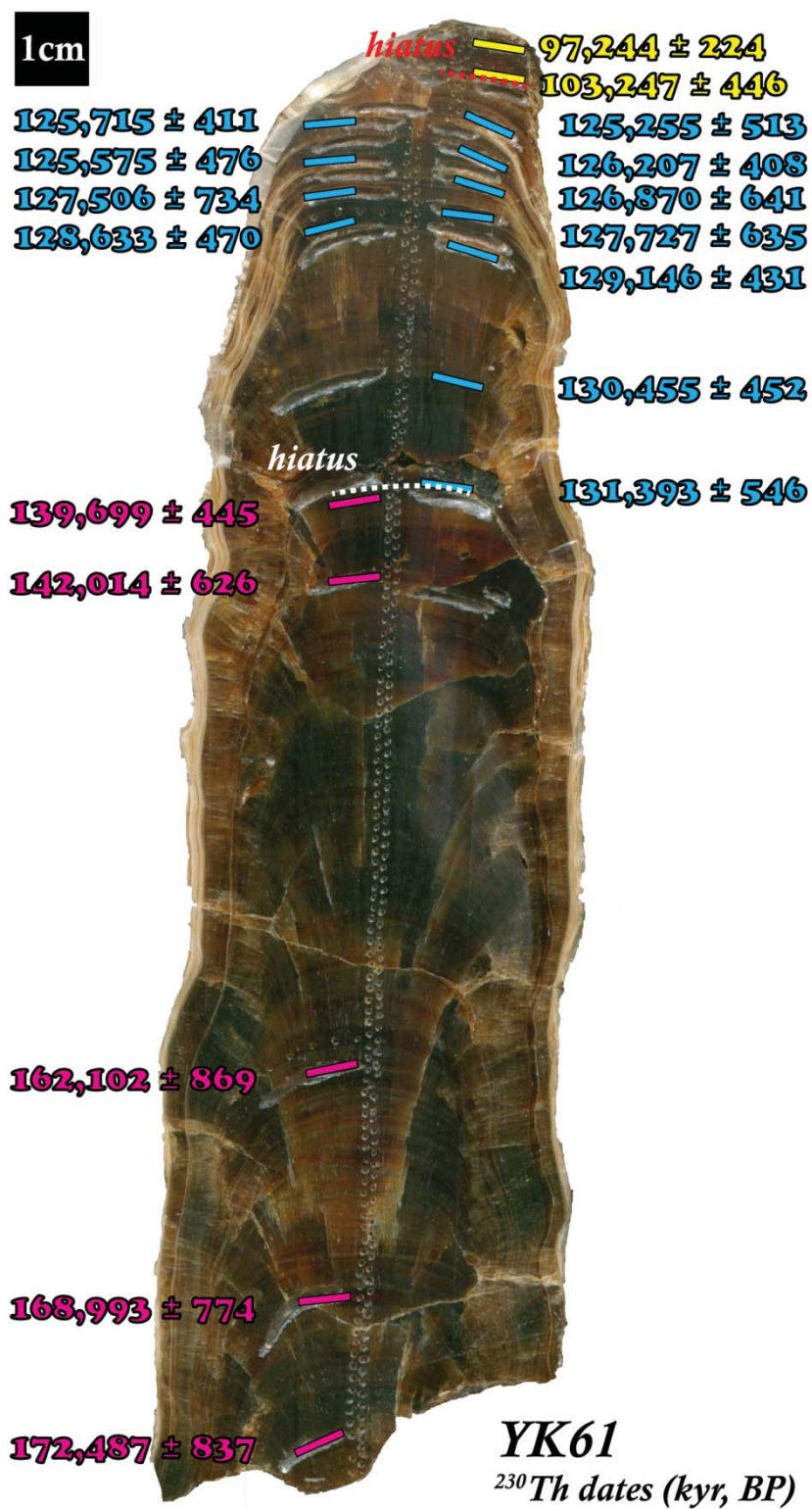
Fig. 3-6   Stalagmite YK61. The solid lines are the [230]Th dating points and the dash

lines are the precipitated hiatus.

3.2 Oxygen isotope records

3.2.1 Hendy Test of Yangkou stalagmites

For each stalagmite, four or more coeval subsamples from two layers at least were arbitrarily chosen for Hendy Test (Hendy, 1971). Hendy Test shows that 1-sigma $\delta^{18}O$ variability of coeval subsamples for all layers are <0.25‰ for YK05, YK12, and YK61 (Fig. 3-7), indicating the stalagmites formed at an oxygen isotopic equilibrium condition and the oxygen isotope data can capture the hydrological signals. The large changes of 0.30‰ for stalagmite YK23 and 0.40‰ for YK47 are probably caused by the difficulty of drilling coeval subsamples on the transitions of oxygen isotope records from the these slow-deposition-rate samples.

Along the growth axes, the poor correlations between $\delta^{18}O$ and $\delta^{13}O$ values for coeval subsamples also indicates no significant kinetic fractionation during carbonate precipitation (Fig. 3-8).
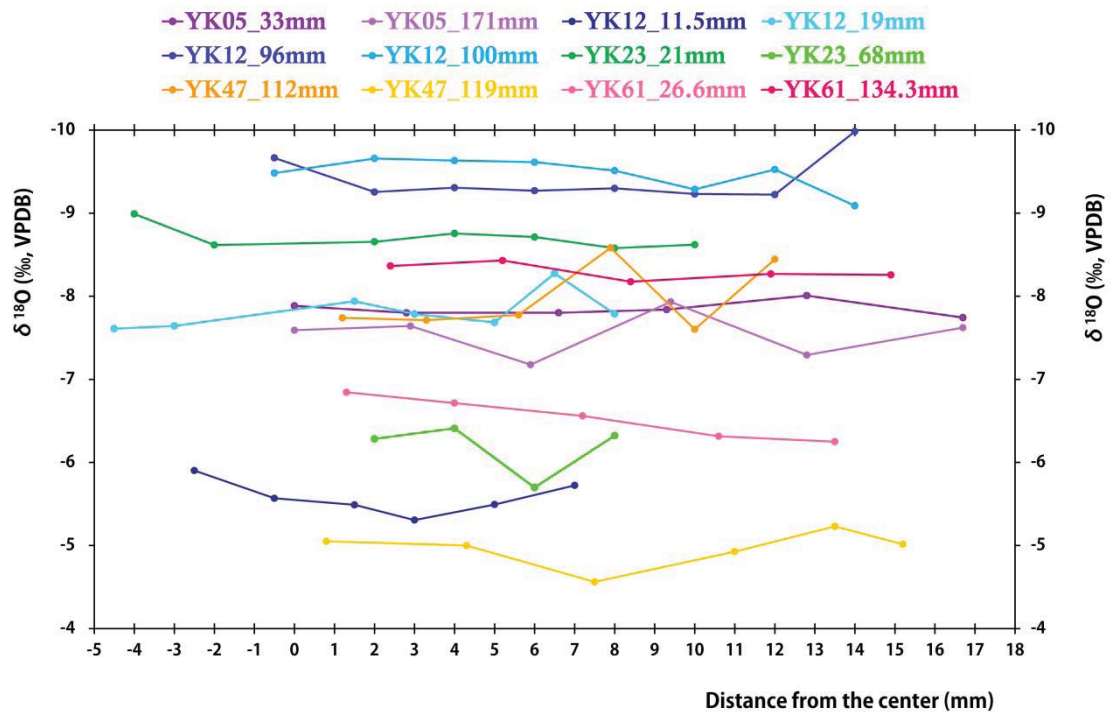
Fig. 3-7　Plots of coeval subsample δ^18O data of the selected 5 stalagmites for Hendy Test.
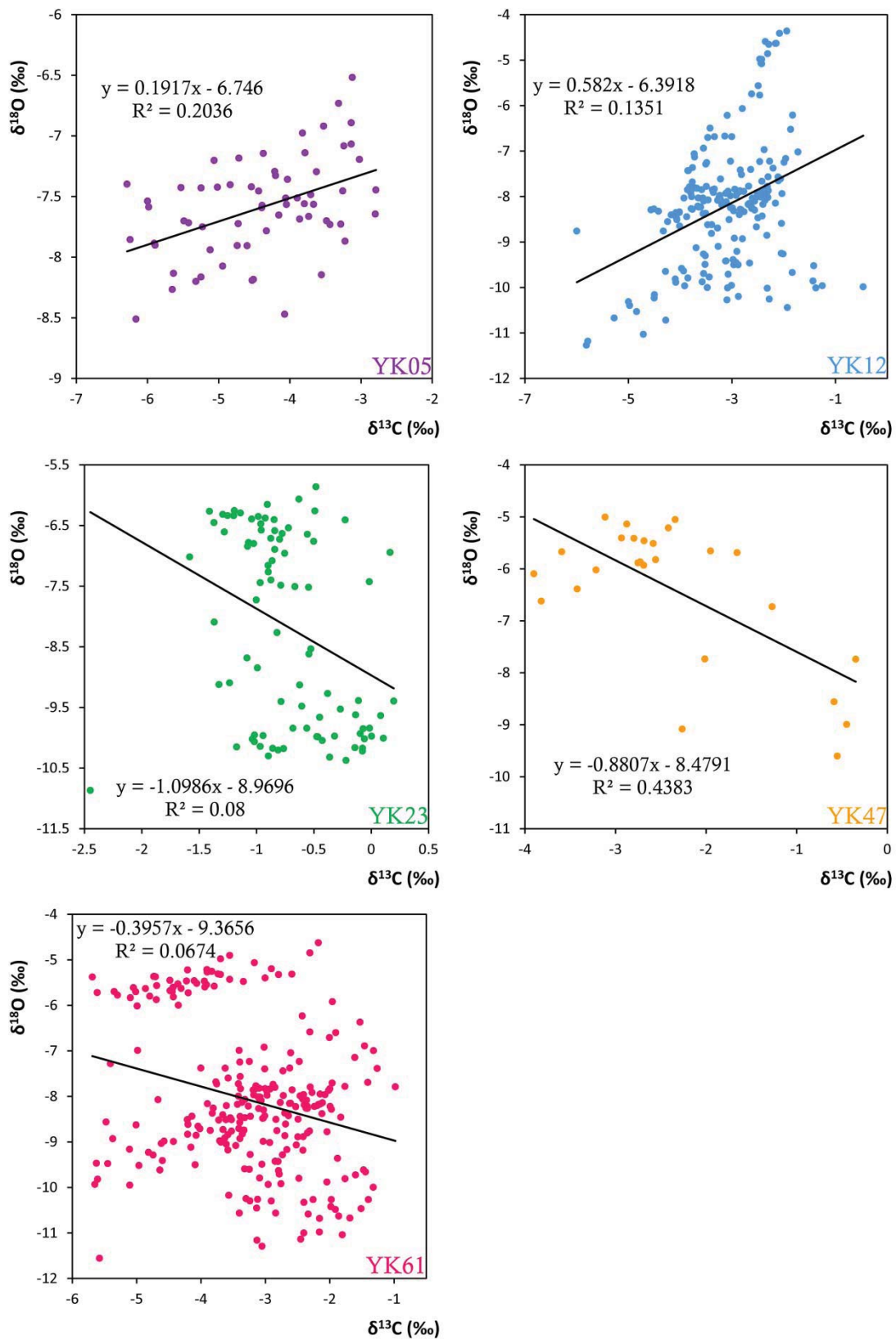
Fig. 3-8 Plots of $\delta^{18}O$ vs. $\delta^{13}C$ for the selected 5 stalagmites show that weak

correlation between $\delta^{18}O$ and $\delta^{13}C$.

3.2.2 Oxygen isotope time series of Yangkou stalagmites

The oxygen isotope sequences of the selected 5 stalagmites are illustrated in Figure 3-9. The spliced record covers a time interval between 124.10-206.46 kyr BP, with three hiatuses of 132.14-133.69 kyr BP, 188.72-193.22 kyr BP, and 198.97-200.83 kyr BP.

Good replication of $\delta^{18}O$ records between stalagmites YK12 and YK61 at an overlapped window of 139-154 kyr BP, combined with sound Hendy Test, indicates stalagmite $\delta^{18}O$ data can represent rainfall oxygen isotopic change and reflect regional hydrological evolution in the AM territory.
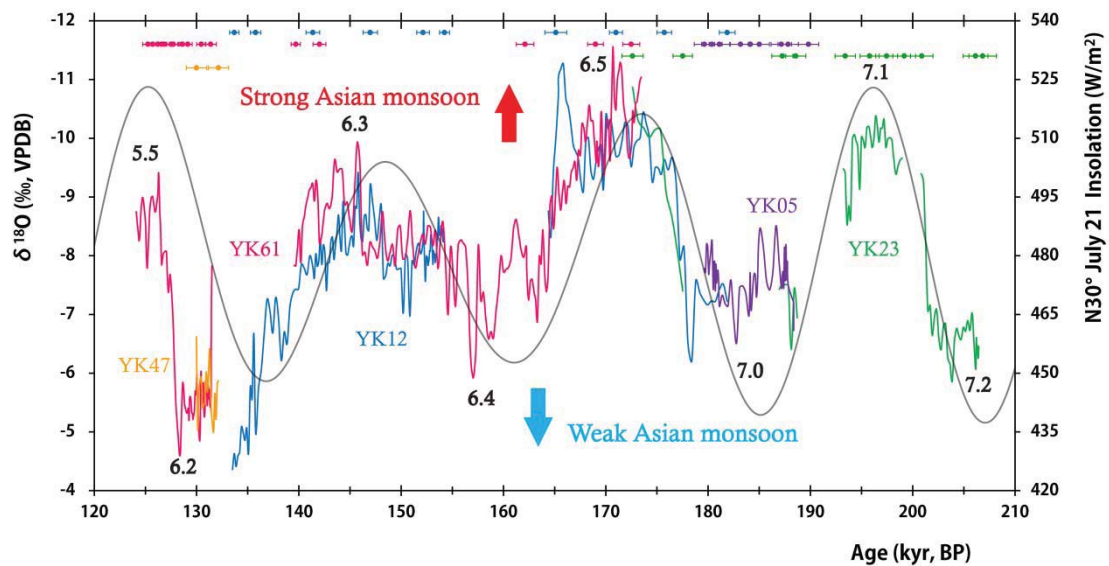
Fig. 3-9 Oxygen isotope records of Yangkou cave stalagmites, YK05 (purple), YK12 (blue), YK23 (green), YK47 (pink), and YK61 (purple). Ages and 2-sigma errors are color-coded by stalagmite. The gray line is the NHSI on 21 July at 30°N,.

3.2.3 δ^{18}O variation of Yangkou stalagmites

The $\delta^{18}O$ values of Yangkou stalagmites during 120-210 kyr BP primarily follow NHSI, including three clear transitions from high to low $\delta^{18}O$ values at 202 kyr BP (between MIS 7.2 and 7.1), 177 kyr BP (between MIS 7.0 and 6.5), and 128 kyr BP (between MIS 6.4 and 6.3). The transition from high to low $\delta^{18}O$ values as well between MIS 6.4 and 6.3 at about 155-148 kyr BP is relatively unclear than the other three. The transitions of $\delta^{18}O$ values from low to high can also be found at 165 kyr BP (between MIS 6.5 and 6.4) and 139 kyr BP (between MIS 6.3 and 6.2).
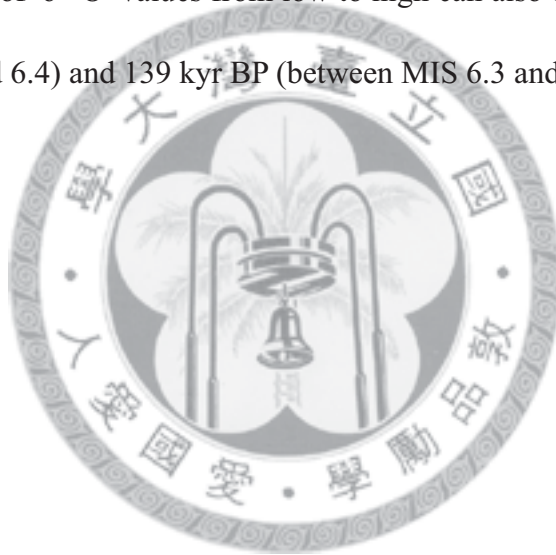
Chapter 4   Discussion

4.1   Comparison with other Chinese caves

Chinese stalagmite ^{18}O records (Cheng et al., 2006; 2009; Wang et al., 2008) have shown that AM intensity primarily follows NHSI on orbital timescales over the past 380 ka (Fig. 1-7). However, the previous researches show that those 100s-kyr records were built with stalagmites mainly from Sanbao Cave only (Wang et al., 2008), which could bring uncertainty in interpreting long-term AM evolution.

A new stalagmite $\delta^{18}O$ sequence from Yangkou cave at a time period of 120-210 ka is highly correlated with previous Chinese ones, including Sanbao cave (Wang et al., 2008), Hulu cave (Cheng et al., 2006), and Dongge cave (Kelly et al., 2006), during MIS 5.5-MIS 7.2 (Fig. 4-1).

Yangkou stalagmite $\delta^{18}O$ records show four strong AM intervals at MIS 5.5 (124-127 kyr, BP), 6.3 (141-148 kyr, BP), 6.5 (165-177 kyr, BP), and 7.1 (193-201 kyr, BP) and four weak AM intervals, MIS 6.2 (128-136 kyr, BP), MIS6.4 (146-164 kyr, BP), MIS 7.0 (178-188 kyr, BP), and MIS 7.2 (201-206 kyr BP) (Fig. 4-1). The consistency among the four caves confirms that the AM events are dominant in the entire mainland and primarily follow NHSI on orbital timescales, (Fig. 4-1), especially the 23-kyr precession cycle (Zachos et al., 2001).

During MIS 6, Yangkou stalagmite-inferred AM sequence superimposes on the

Sanbao record, which confirms that the AM events, including the weakest one at the penultimate deglaciation (MIS 6.2; 128-136 ka) and the strongest one at MIS 6.5 during 166-177 ka, are dominant in the entire mainland and primarily follow NHSI on precessional orbital timescales.

Our results show that the transition event of Yankou cave between MIS 6.2 and 5.5 occurred in 128 kyr (BP) which is about 1 kyr later than the same event of Sanbao, Hulu, and Dongge cave which happened in 129 kyr (BP). The inconsistency is still the unsolved puzzle here.
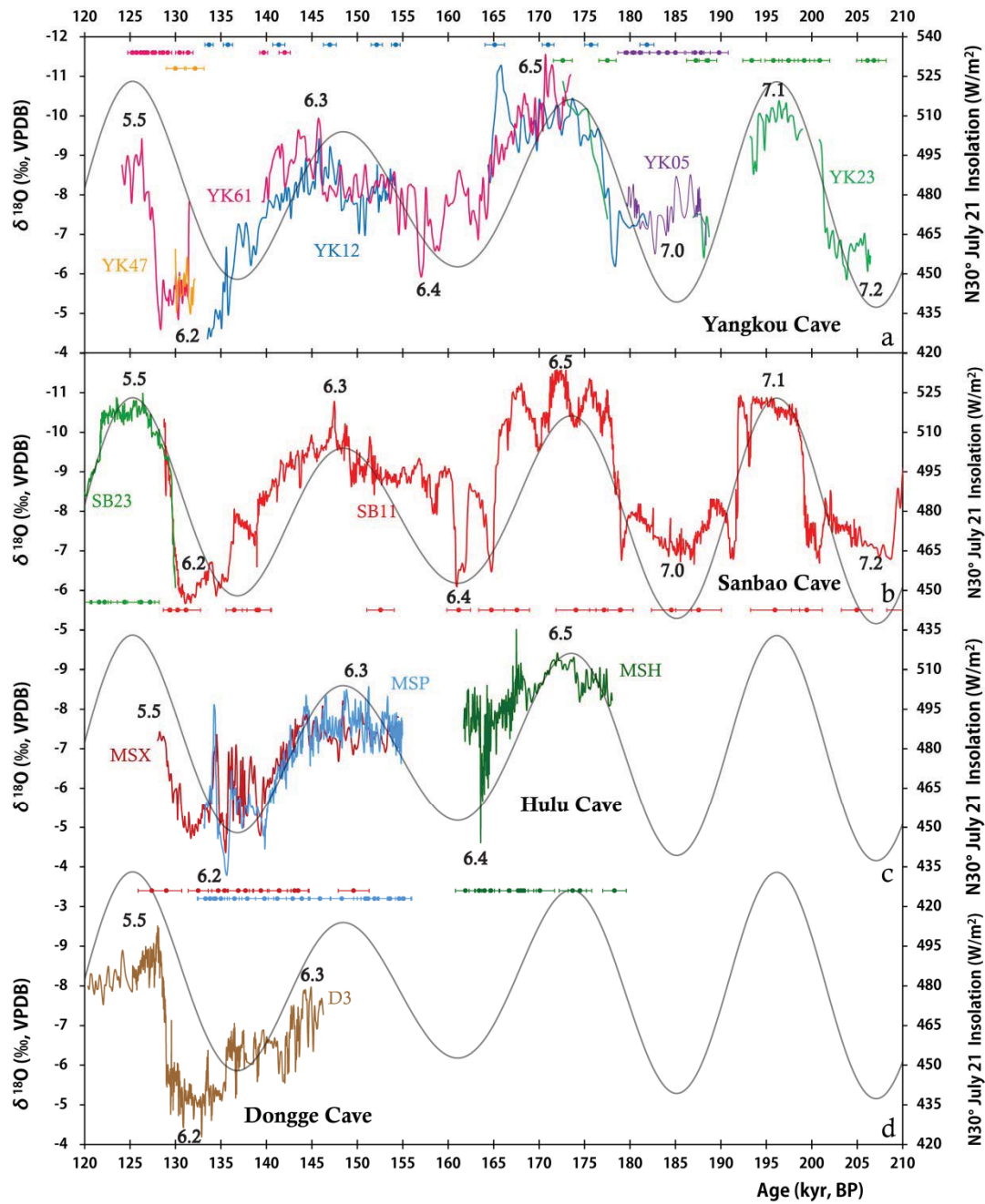
Fig. 4-1   Comparison of stalagmites $\delta^{18}O$ records among 120-210 ka from Chinese

caves, including (a) Yangkou $\delta^{18}O$ (this study), (b) Sanbao (Wang et al.,

2008), (c) Hulu (Cheng et al., 2006), and (d) Dongge (Kelly et al., 2006). The

gray line is the NHSI on 21 July at 30°N. ^{230}Th dates and 2-sigma errors are

color-coded by stalagmite.

4.2   AM forcings at different time windows

4.2.1   Glacial/interglacial period

Magnetic susceptibility records of loess can be one of paleoproxies for AM intensity (Sun et al., 2006; Cheng et al., 2012). High magnetic susceptibility of loess relates to the strong AM intensity (wet period), whereas the low magnetic susceptibility of loess relates to the weak AM intensity (dry period). The loess-inferred AM intensity highly correlates to the glacial/interglacial periods represented in the LR04 benthic foraminiferal stack $\delta^{18}O$ records (Lisiecki and Raymo, 2005; Sun et al., 2006; Cheng et al., 2012) (Fig. 4-2d & e). However, this glacial/interglacial correlation cannot be found in East Asian cave $\delta^{18}O$ records (Fig. 4-2a). Low magnetic susceptibility records of Lingtai and Zhaojiachuan loess suggest a whole weak AM interval during MIS 6 (Sun et al., 2006), which conflicts with two strong AM intervals at MIS 6.3 and 6.5 illustrated in the previous East Asian stalagmite records (Cheng et al., 2006; Kelly et al., 2006; Wang et al., 2008).

The inconsistency could be caused by two possibilities: (1) The loess records could be less sensitive for ASM boundary than the current Chinese stalagmites. (2) The dispute may be explained by northwest boundary shift of the ASM. During the glacial period, such as MIS 2, 4, 6, or 8, the ice volume on the northern Eurasia, Greenland, and America extended (Solomon et al., 2007; Stauch and Lehmkuhl, 2010), enhancing the Siberian high and pushing the northwest boundary of ASM southeastward. During

the interglacial period, the ice volume shrank, the Siberian high was weakened, and

ASM boundary shifted northward. The location of Lingtai and Zhaojiachuan loess (Sun

et al., 2006) is in the north of Yangkou, Sanbao, Hulu, and Dongge caves (Cheng et al.,

2006; Kelly et al., 2006; Wang et al., 2008) (Fig. 2-1). The different responses between

caves and loess could be attributed to that the location of ASM northwest boundary,

which might be in the middle region between Sanbao cave and Lingtai and

Zhaojiachuan loess during MIS 6 (Fig. 4-3). The locations of the Chinese caves have

been more sensitive than loess.

The 2nd proposed possibility can be supported by Kensang cave study (Cheng et

al., 2012) . The monsoon intensity inferred from Kensang stalagmites is weaker than

that from Lingtai and Zhaojiachuan loess during MIS 6, likely resulting from different

localities. It is difficult for the ASM front to reach Kensang cave, located in Central

Asian, northwest of Lingtai and Zhaojiachuan loess sites.
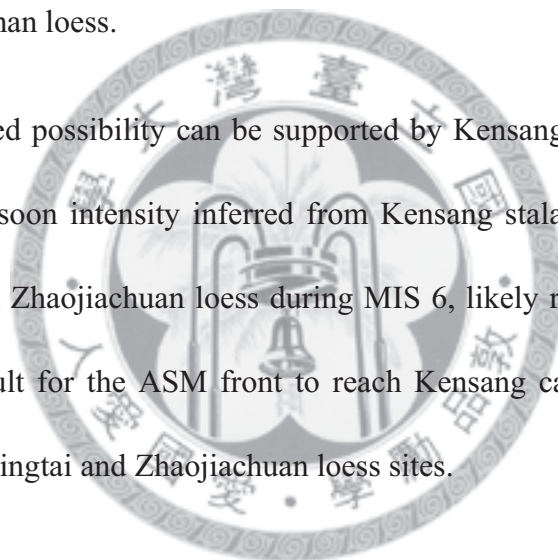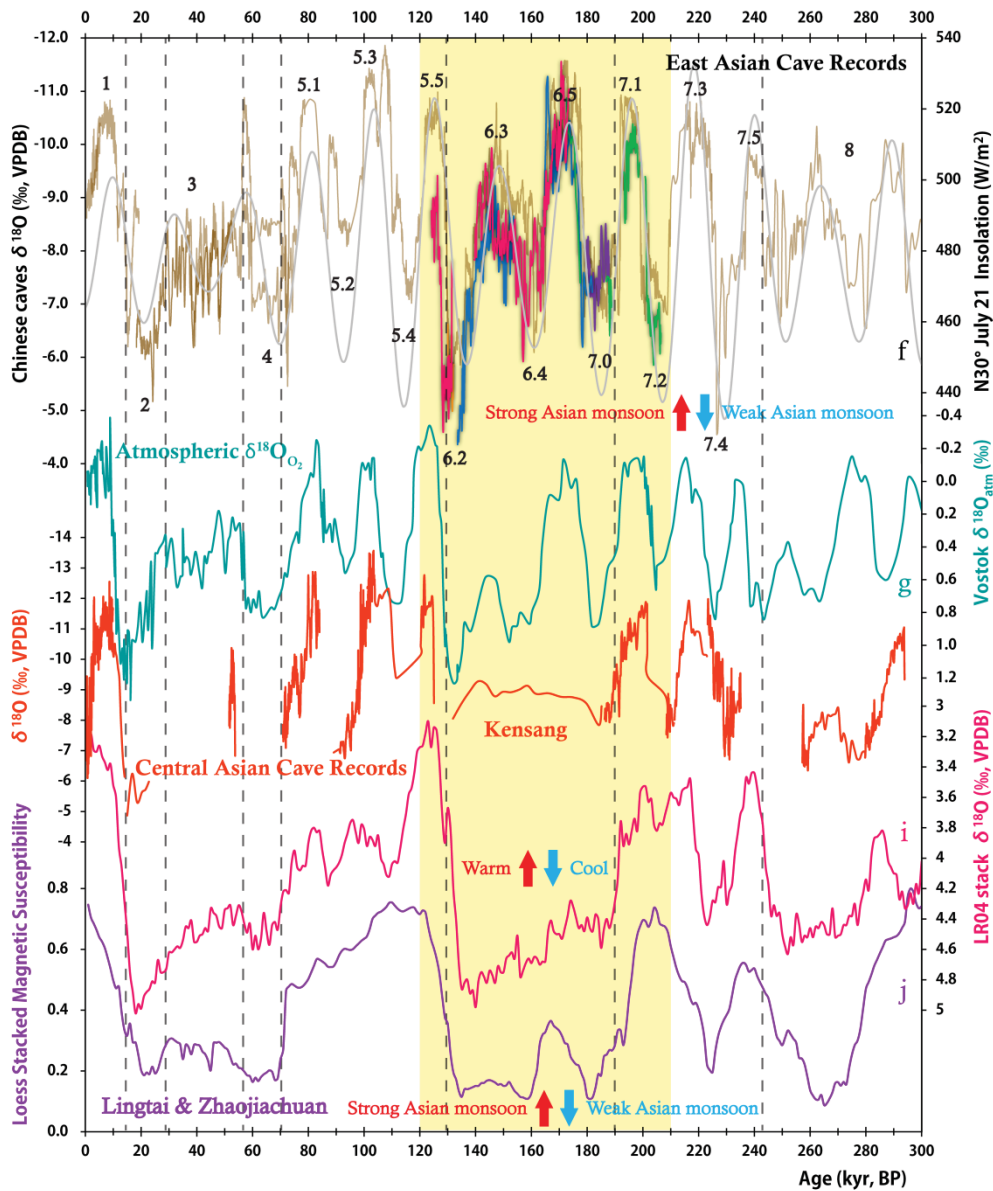
Fig. 4-2 (a) $\delta^{18}O$ records of Yangkou cave. Light brown line is a composite record of

$\delta^{18}O$ data from previous East Asian cave studies (Cheng et al., 2006; 2009;

Wang et al., 2008). Gray curve is the NHSI on 21 July at 30°N. (b)

Atmospheric $\delta^{18}O$ variation from Vostok ice core, Antarctica (Sowers et al.,

1991; Petit et al., 1999). (c) $\delta^{18}O$ records of Kensang cave located in Central

Asian (Cheng et al., 2012). (d) LR04 Benthic Stack $\delta^{18}O$ record, reflecting

global ice volume (Lisiecki and Raymo, 2005). (e) Loess magnetic

susceptibility records of Lingtai and Zhaojiachuan (Sun et al., 2006).
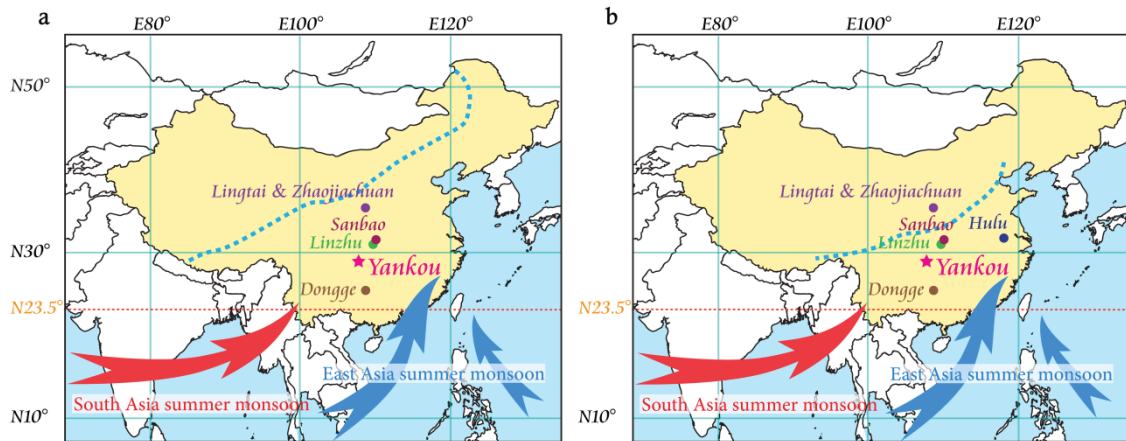
Fig. 4-3　(a) Locations of Chinese caves (Yangkou, Sanbao, Linzhu, Hulu, and Dongge) (Wang et al., 2001; Kelly et al., 2006; Cheng et al., 2006;Wang et al., 2008; Cheng et al., 2009) and loess sites (Lingtai and Zhaojiachuan) (Sun et al., 2006). The blue dashed line represents the approximate northern extent of the ASM (Kelly et al., 2000). (b) During MIS 6, the northwest boundary of ASM might shift southeastward to a region between the locations of Sanbao cave and Lingtai and Zhaojiachuan loess.

4.2.2　Abnormal strong ASM at MIS 6.5

One striking feature of stalagmite-inferred ASM during MIS 5-7 is an extraordinarily strong period at MIS 6.5 with $\delta^{18}O$ values even lower than those at interglacial events of MIS 5.5 or 7.3 (Fig. 4-1). Wang et al. (2008) found that there is a good correlation between the stalagmite-inferred AM intensity and the atmospheric $\delta^{18}O$ ($\delta^{18}O_{atm}$) records from Antarctic Vostok ice core O_2 bubbles (Sowers et al., 1991 ;Petit et al., 1999; Wang et al., 2008) (Fig. 1-8). Wang et al. (2008) suggested the Dole effect can explain this similarity (Dole, 1936; Bender et al., 1994).

Dole effect was first described by Dole in 1936. This effect is an inequality of $\delta^{18}O$ values between the atmosphere and seawater. Modern $\delta^{18}O_{atm}$ is ~23.5‰ (±0.3‰) heavier than seawater value (Kroopnick and Craig, 1972). This inequality is caused by respiration which prefers depleting $^{16}O_2$ in the atmosphere rather than $^{18}O_2$. On the other hand, the inequality can be balanced by photosynthesis, which emits the oxygen with the $\delta^{18}O$ value equal to the water used in the reaction (Guy et al., 1989) which can decrease atmospheric $\delta^{18}O$ value. Hence, the $\delta^{18}O$ variation of the atmospheric O_2 can depend on the activity of photosynthesis.

Vostok ice core-inferred $\delta^{18}O_{atm}$ evolution likely results from changes of summer insolation and rainfall amount in NH, where land provides space for growth of vegetation and intense photosynthesis. The extraordinarily strong ASM with high precipitation intensity at MIS 6.5 with low summer insolation could be attributed to an additional forcing.
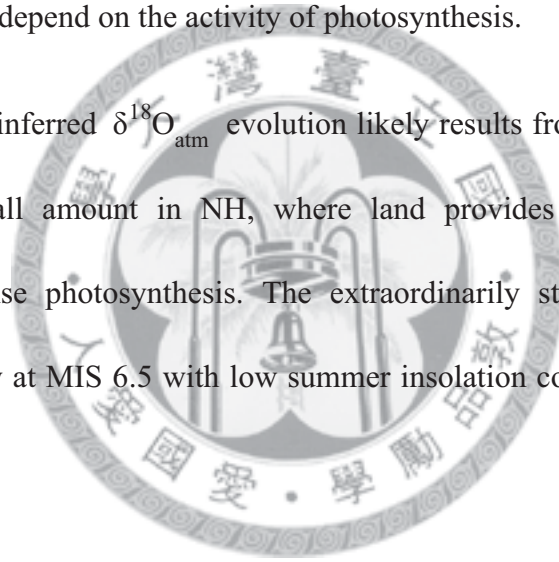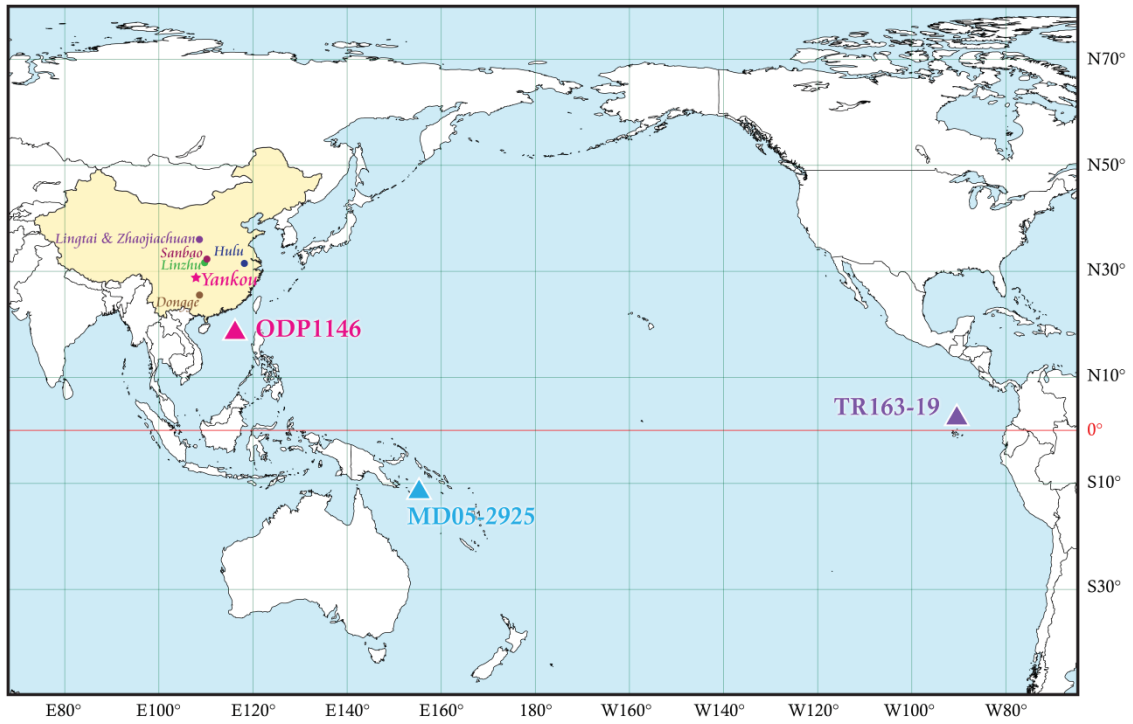
Fig. 4-4　Sites of TR163-19 (purple; triangle) (Lea et al., 2000), MD05-2925 (blue;

triangle) (Chang, 2012), and ODP1146 (pink; triangle) (Clemens and Prell,

2003).
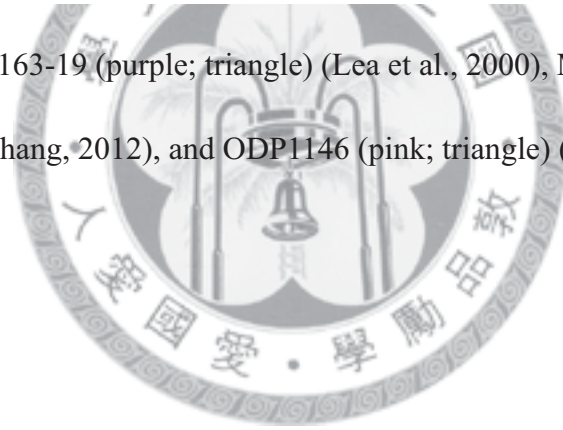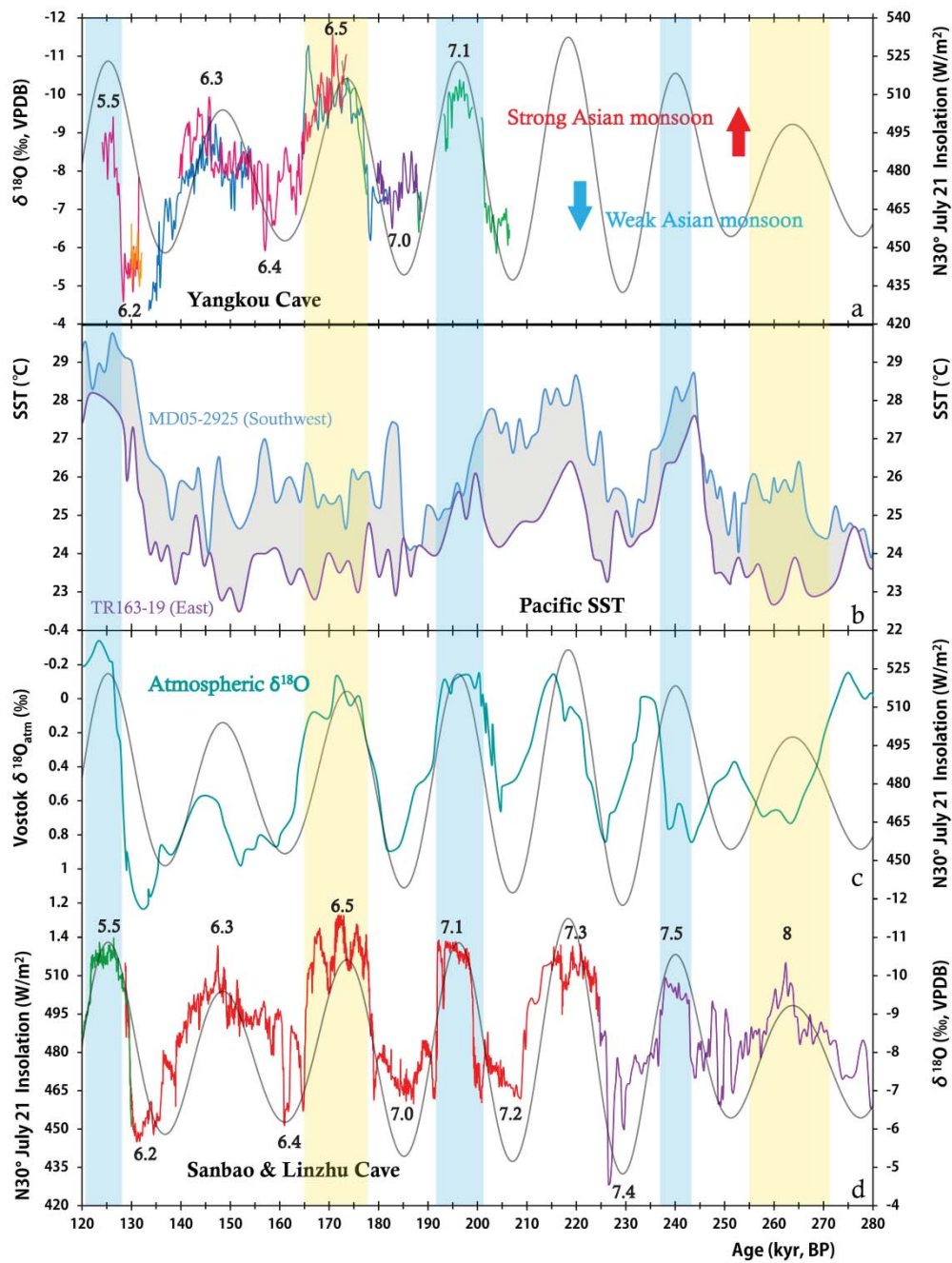
Fig. 4-5　(a) Yangkou stalagmite $\delta^{18}O$ records. (b) Reconstructed EEP (purple, core

TR163-19, Lea et al., 2000) and SPWP (blue, core MD05-2925, Chang, 2012)

Pacific SSTs. The gray zones denote large SSTD between the two sites. (c)

Sanbao and Linzhu stalagmite $\delta^{18}O$ records (Wang et al., 2008; Cheng et al.,

2009). (d) Atmospheric $\delta^{18}O$ record from Vostok ice core, Antarctica

(Sowers et al., 1991; Petit et al., 1999).

Stalagmite $\delta^{18}O$ records of Yangkou, Sanbao, and Linzhu caves (Wang et al., 2008; Cheng et al., 2009) and also Pacific sea surface temperature (SST) in the southwestern Pacific warm pool (SPWP) (Chang, 2012) and TR163-19 in the eastern equatorial Pacific (EEP) (Lea et al., 2000) are plotted in Figure 4-5. SST difference (SSTD) between SPWP and EEP at MIS 6.5 is larger (Fig. 4-5; yellow zone) than those at MIS 5.5 and 7.1 (Fig. 4-5; blue zone). This large SSTD could be attributed to an enhanced Walker circulation in the tropical Pacific. The strong Walker circulation, called as a La Niña-like event (Fig. 4-8a, right), could move the rainfall zone westward and enhance ASM precipitation in East Asia (Clement et al., 1999). Whereas, under a weak Walker circulation, analog to a El Niño-like condition (Fig. 4-8a, left), rainfall zone in the Pacific migrate eastward and EAM precipitation was reduced (Clement et al., 1999).

The sea water $\delta^{18}O$ records ($\delta^{18}O_w$) of ODP1146 and MD05-2925, representing the salinity variation of South China Sea (SCS) and SPWP, also show that the intervals with strong ASM are featured with low-salinity and wet conditions in the western Pacific (Fig. 4-7).

These arguments are supported with modern meteorological observations of that La Niña events accompany the probability of precipitation above normal in China (Fig. 4-8b) (IRI, 2008). Linzhu stalagmite-inferred strong ASM at MIS 8 (Cheng et al., 2009) could also result from a strong Walker circulation with large SSTD between western and eastern Pacific (Fig. 4-5).

Meteorological rainfall records during 1953-2010 at Yichang (~150km southeast of Sanbao cave) and Zunyi (~150km south of Yangkou) express different mean summer rainfall between El Niño and La Niña years (CMA, 2012). During April to October, the mean rainfall was larger in La Niña years than El Niño years (Fig. 4-6).
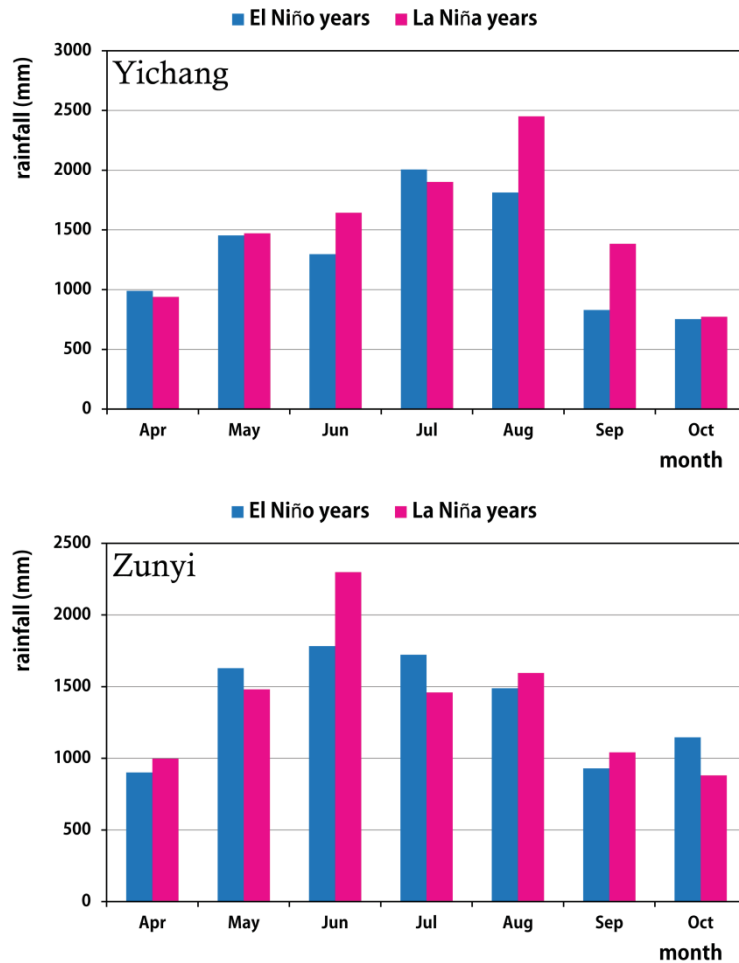
Fig. 4-6   Mean rainfall records of Yichang and Zunyi during April to October in 1953-2010 (CMA, 2012). The pink histograms refer to La Niña years, 1954, 1955, 1956, 1964, 1971, 1973, 1974, 1985, 1988, 1998, 1999, 2000, and 2010. The blue bars are El Niño years of 1953, 1957, 1963, 1965, 1969, 1972, 1982, 1987, 1991, 1997, and 2002.
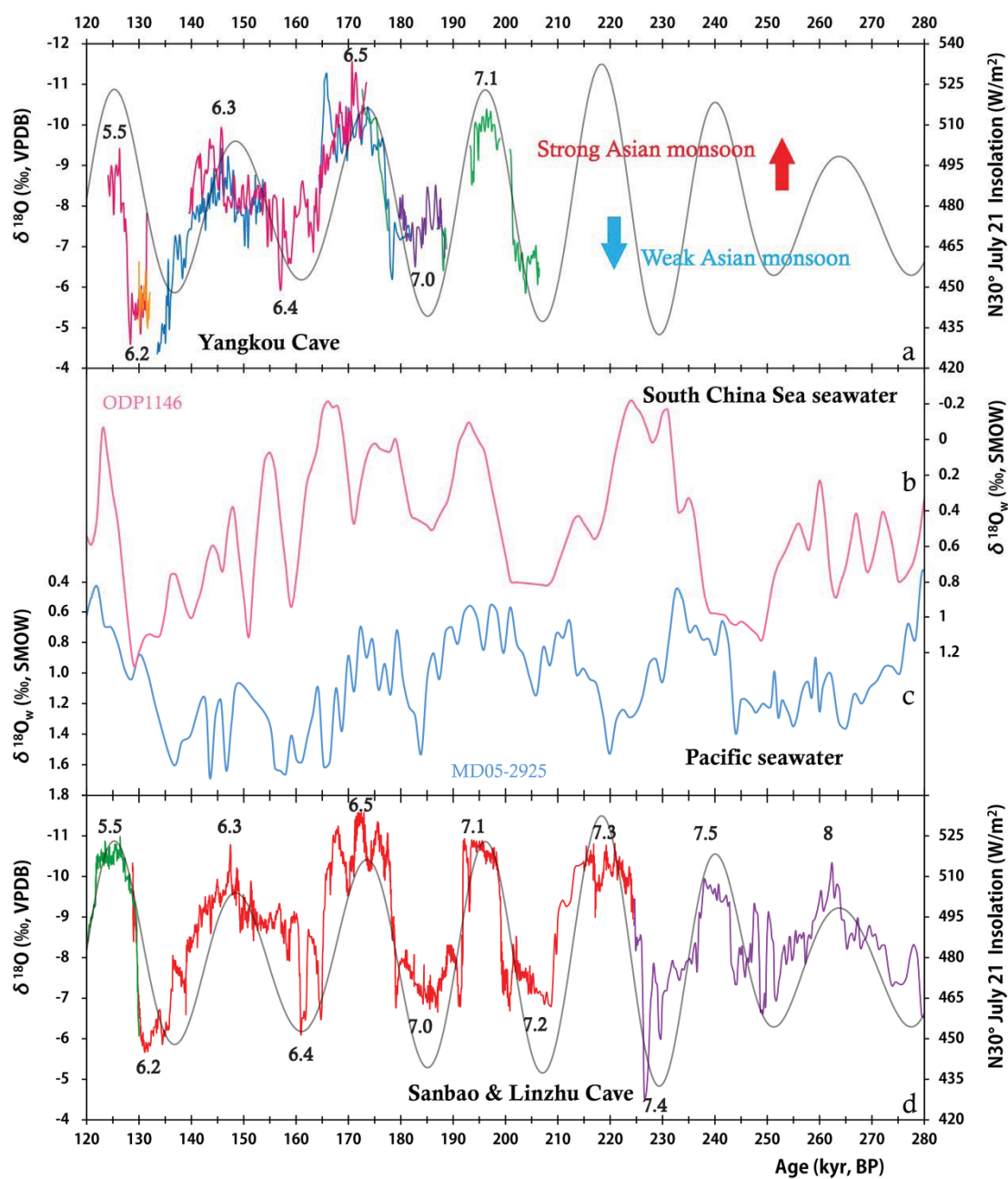
Fig. 4-7 (a) Yangkou $\delta^{18}O$ records. $\delta^{18}O_w$ records of (b) core ODP1146 from SCS (Clemens and Prell, 2003) and (c) core MD05-2925 from southwestern tropical Pacific Ocean (Chang, 2012). (d) Sanbao and Linzhu stalagmite $\delta^{18}O$ records (Wang et al., 2008; Cheng et al., 2009).

a

weak Walker circulation (El Niño-like)

b

strong Walker circulation (La Niña-like)

c

Precipitation Above Normal

El Niño

La Niña

Precipitation Below Normal

El Niño

La Niña

Frequency of Occurence   Low   High
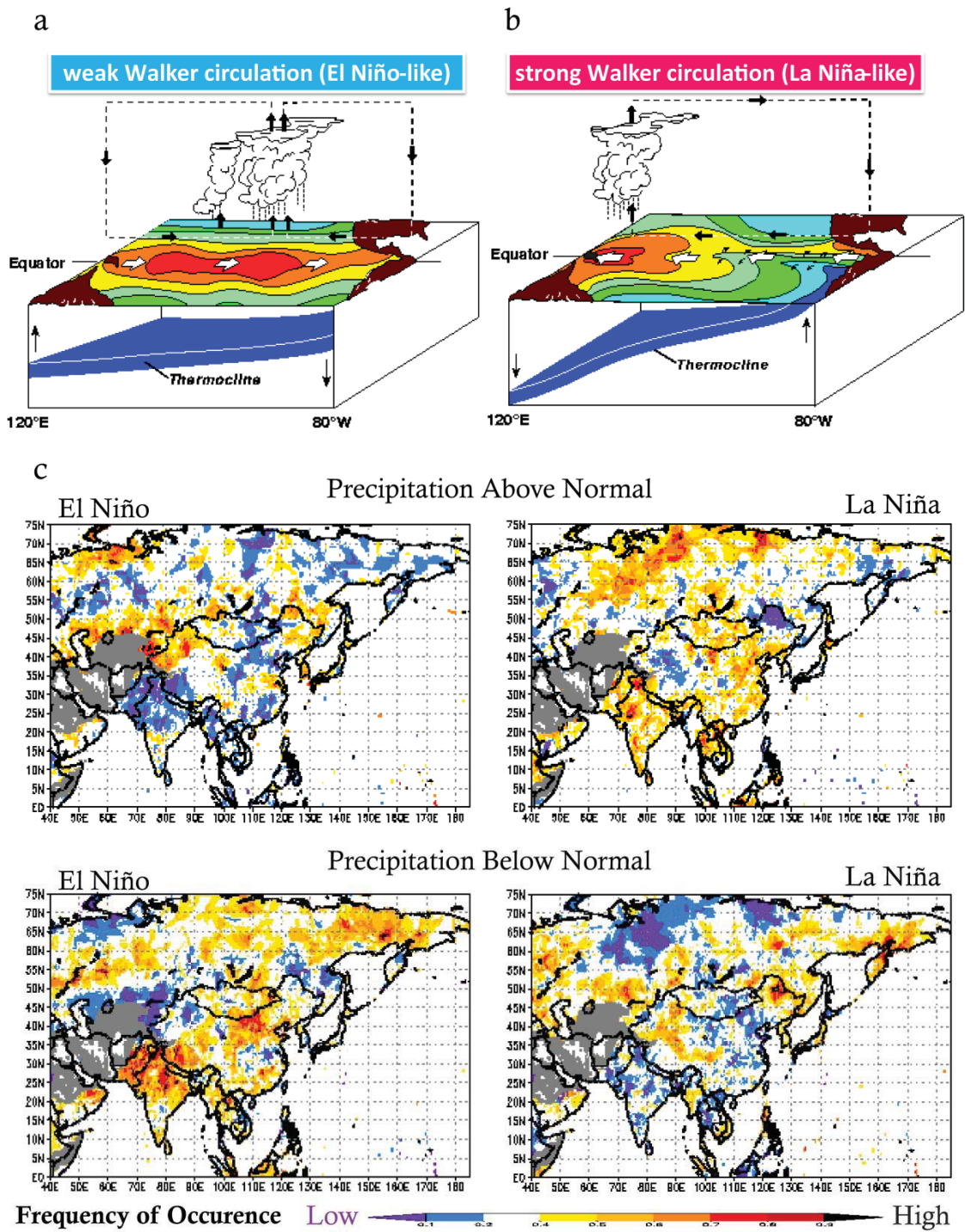
Fig. 4-8   (a) Modern weak Walker circulation during El-Niño events and (b) strong

Walker circulation during La-Niña events (Clement et al., 1999; NOAA,

2012). (c) Precipitation probability in Euro-Asia region during El-Niño (left)

and La-Niña (right) events based on modern observations during AD

1950-1995 (IRI, 2008).

Chapter 5 Conclusions

Previous Chinese cave studies (Cheng et al., 2006; 2009;Wang et al., 2008) showed that AM intensity primarily follows NHSI on orbital timescales over the past 380 kyr BP. However, during MIS 6, the Asian monsoon variation had been reconstructed mainly from Sanbao cave (Wang et al., 2008) which brings tremendous uncertainties in interpreting long-term AM records. The agreement of our new δ^{18}O records from Yangkou cave with other caves in the mainland China during 124-206 kyr BP at MIS 6-7 confirms that the AM events, including the weakest one at the penultimate deglaciation (MIS 6.2; 128-136 ka) and the strongest one at MIS 6.5 during 166-177 ka, are dominant in the entire mainland and primarily follow NHSI on precessional orbital timescales.

During MIS 6, Yangkou stalagmite-inferred AM variations are consistent with other Chinese caves records but conflict with the loess data. This disagreement could be attributed to the southeastward of ASM boundary during the glacial time. The consistency between stalagmite-inferred ASM and Vostok atmospheric δ^{18}O time series suggests an additional ASM forcing, which could be the glacial/interglacial dynamics of Walker circulation in the tropical Pacific.

References

An, Z. (2000), The history and variability of the East Asian paleomonsoon climate, Quaternary Science Reviews, 19(1–5), 171-187.

An, Z., et al. (2011), Glacial-Interglacial Indian Summer Monsoon Dynamics, Science, 333(6043), 719-723.

Bender, M., T. Sowers, and L. Labeyrie (1994), The Dole Effect and its variations during the last 130,000 years as measured in the Vostok Ice Core, Global Biogeochem. Cycles, 8(3), 363-376.

Chang, S.-P. (2012), Sea surface temperature record at the Southern Margin of the Western Pacific Warm Pool over the past 360 kyrs, National Taiwan University, Taipei.

Cheng, H., R. L. Edwards, Y. Wang, X. Kong, Y. Ming, M. J. Kelly, X. Wang, C. D. Gallup, and W. Liu (2006), A penultimate glacial monsoon record from Hulu Cave and two-phase glacial terminations, Geology, 34(3), 217-220.

Cheng, H., R. L. Edwards, W. S. Broecker, G. H. Denton, X. Kong, Y. Wang, R. Zhang, and X. Wang (2009), Ice Age Terminations, Science, 326(5950), 248-252.

Cheng, H., P. Z. Zhang, C. Spötl, R. L. Edwards, Y. J. Cai, D. Z. Zhang, W. C. Sang, M. Tan, and Z. S. An (2012), The climatic cyclicity in semiarid-arid central Asia over the past 500,000 years, Geophys. Res. Lett., 39(1), L01705.

Clemens, S. C., and W. L. Prell (2003), Data Report: Oxygen and Carbon Isotopes from Site 1146, Northern South China Sea, Scientific Results, 184, 1-8.

Clement, A. C., R. Seager, and M. A. Cane (1999), Orbital Controls on the El

Niño/Southern Oscillation and the Tropical Climate, Paleoceanography, 14(4),

441-456.

CMA (2012), China Meteorological Administration meteorological records,

http://www.cma.gov.cn/, edited.

Dansgaard, W. (1964), Stable isotopes in precipitation, Tellus, 16(4), 436-468.

Dole, M. (1936), The Relative Atomic Weight of Oxygen in Water and in Air A

Discussion of the Atmospheric Distribution of the Oxygen Isotopes and of the

Chemical Standard of Atomic Weights, The Journal of Chemical Physics, 4(4),

268-275.

Dykoski, C. A., R. L. Edwards, H. Cheng, D. Yuan, Y. Cai, M. Zhang, Y. Lin, J. Qing, Z.

An, and J. Revenaugh (2005), A high-resolution, absolute-dated Holocene and

deglacial Asian monsoon record from Dongge Cave, China, EPSL, 233(1-2),

71-86.

Fairchild, I. J., C. L. Smith, A. Baker, L. Fuller, C. Spötl, D. Mattey, F. McDermott, and

E.I.M.F (2006), Modification and preservation of environmental signals in

speleothems, Earth-Science Reviews, 75(1–4), 105-153.

Faure, G. (1986), Principle of isotope Geology, 2 ed., Wiley.

Faure, G. (1998), Principles of Applications of Geochemistry, 2 ed., Prentice Hall.

Fleitmann, D., S. J. Burns, U. Neff, A. Mangini, and A. Matter (2003), Changing

moisture sources over the last 330,000 years in Northern Oman from

fluid-inclusion evidence in speleothems, Quaternary Research, 60(2), 223-232.

Fleitmann, D., S. J. Burns, U. Neff, M. Mudelsee, A. Mangini, and A. Matter (2004), Palaeoclimatic interpretation of high-resolution oxygen isotope profiles derived from annually laminated speleothems from Southern Oman, Quaternary Science Reviews, 23(7–8), 935-945.

Gonfiantini, R., M.-A. Roche, J.-C. Olivry, J.-C. Fontes, and G. M. Zuppi (2001), The altitude effect on the isotopic composition of tropical rains, Chemical Geology, 181(1–4), 147-167.

Guy, R. D., J. A. Berry, M. L. Fogel, and T. C. Hoering (1989), Differential fractionation of oxygen isotopes by cyanide-resistant and cyanide-sensitive respiration in plants, Planta, 177(4), 483-491.

Hendy, C. H. (1971), The isotopic geochemistry of speleothems—I. The calculation of the effects of different modes of formation on the isotopic composition of speleothems and their applicability as palaeoclimatic indicators, Geochimica et Cosmochimica Acta, 35(8), 801-824.

IRI (2008), Statistical Climate Prediction Tool: Probabilistic Composites Keyed to ENSO, http://iri.columbia.edu/climate/forecast//enso/index.html, edited, IRI.

Kelly, M. J., R. L. Edwards, H. Cheng, D. X. Yuan, Y. J. Cai, M. L. Zhang, Y. S. Lin, and Z. S. An (2006), High resolution characterization of the Asian Monsoon between 146,000 and 99,000 years BP from Dongge Cave, China and global correlation of events surrounding Termination II, PPP, 236(1-2), 20-38.

Kim, S.-T., and J. R. O'Neil (1997), Equilibrium and nonequilibrium oxygen isotope effects in synthetic carbonates, Geochimica et Cosmochimica Acta, 61(16),

3461-3475.

Kroopnick, P., and H. Craig (1972), Atmospheric Oxygen: Isotopic Composition and

Solubility Fractionation, Science, 175(4017), 54-55.

Lea, D. W., D. K. Pak, and H. J. Spero (2000), Climate Impact of Late Quaternary

Equatorial Pacific Sea Surface Temperature Variations, Science, 289(5485),

1719-1724.

Li, T.-Y., et al. (2011), Oxygen and carbon isotopic systematics of aragonite

speleothems and water in Furong Cave, Chongqing, China., Geochim. Cosmochim.

Acta, 75, 4140-4156.

Lisiecki, L. E., and M. E. Raymo (2005), A Pliocene-Pleistocene stack of 57 globally

distributed benthic δ18O records, Paleoceanography, 20(1), PA1003.

M.Baum, E., H. D. Knox, and T. R. Miller (2002), Nuclides and Isotopes : Chart of the

Nuclides, 16 ed., Lockheed MartinKnolls.

NOAA (2012), NOAA's El Niño Page, http://www.elnino.noaa.gov/index.html, edited.

O'Neil, J. R., R. N. Clayton, and T. K. Mayeda (1969), Oxygen Isotope Fractionation in

Divalent Metal Carbonates, The Journal of Chemical Physics, 51(12), 5547-5558.

Petit, J. R., et al. (1999), Climate and atmospheric history of the past 420,000 years

from the Vostok ice core, Antarctica, Nature, 399(6735), 429-436.

Rozanski, K., Aragu, aacute, A. s, L. s, and R. Gonfiantini (1993), Isotopic patterns in

modern global precipitation, in Climate Change in Continental Isotopic Records,

edited, pp. 1-36, AGU, Washington, DC.

Shen, C.-C., et al. (2012), U-Th isotopic determinations in femtogram quantities and

High-precision and high-resolution carbonate 230Th dating by MC-ICP-MS with SEM protocols, GCA (in review).

Shen, C.-C., et al. (2008), Variation of initial 230Th/232Th and limits of high precision U–Th dating of shallow-water corals, Geochimica et Cosmochimica Acta, 72(17), 4201-4223.

SINA (2010), Meteorological statistics of Mt. Jinfo, Chongqing, http://php.weather.sina.com.cn/whd.php?city=%BD%F0%B7%F0%C9%BD&m=1&dpc=1, edited, SINA Corporation.

Solomon, S., D. Qin, M. Manning, M. Marquis, K. Averyt, M. M. B. Tignor, J. Henry LeRoy Miller, and Z. Chen (2007), Contribution of Working Group I to the Fourth Assessment Report of the Intergovernmental Panel on Climate Change, Cambridge University Press.

Sowers, T., M. Bender, D. Raynaud, Y. S. Korotkevich, and J. Orchardo (1991), The δ18O of Atmospheric O2 from Air Inclusions in the Vostok Ice Core: Timing of CO2 and Ice Volume Changes During the Penultimate Deglaciation, Paleoceanography, 6(6), 679-696.

Stauch, G., and F. Lehmkuhl (2010), Quaternary glaciations in the Verkhoyansk Mountains, Northeast Siberia, Quaternary Research, 74(1), 145-155.

Sun, Y., S. C. Clemens, Z. An, and Z. Yu (2006), Astronomical timescale and palaeoclimatic implication of stacked 3.6-Myr monsoon records from the Chinese Loess Plateau, Quaternary Science Reviews, 25(1–2), 33-48.

Wang, X., A. S. Auler, R. L. Edwards, H. Cheng, E. Ito, and M. Solheid (2006),

Interhemispheric anti-phasing of rainfall during the last glacial period, Quaternary Science Reviews, 25(23-24), 3391-3403.

Wang, Y., H. Cheng, R. L. Edwards, X. Kong, X. Shao, S. Chen, J. Wu, X. Jiang, X. Wang, and Z. An (2008), Millennial- and orbital-scale changes in the East Asian monsoon over the past 224,000 years, Nature, 451(7182), 1090-1093.

Wang, Y. J., H. Cheng, R. L. Edwards, Z. S. An, J. Y. Wu, C.-C. Shen, and J. A. Dorale (2001), A High-Resolution Absolute-Dated Late Pleistocene Monsoon Record from Hulu Cave, China, Science, 294(5550), 2345-2348.

Zachos, J., M. Pagani, L. Sloan, E. Thomas, and K. Billups (2001), Trends, Rhythms, and Aberrations in Global Climate 65 Ma to Present, Science, 292(5517), 686-693.

Zhang, P., et al. (2008), A Test of Climate, Sun, and Culture Relationships from an 1810-Year Chinese Cave Record, Science, 322(5903), 940-942.

Zhao, K., Y. Wang, R. L. Edwards, H. Cheng, and D. Liu (2010), High-resolution stalagmite $\delta18O$ records of Asian monsoon changes in central and southern China spanning the MIS 3/2 transition, EPSL, 298(1-2), 191-198.

Appendix I   labware cleaning processes

※ **During the acid-cleaning procedure, beakers with acid should never leave fume hood.**

※ **While touching any warm glass beaker or pouring warm acid from a glass beaker, operator must wear apron, face shield, and long rubber gloves.**

※ **After using any glass beaker, clean it with H_2O and pour into sink with copious amounts of tap water, and then keep it on shelf with empty.**

Teflonware (reusable)

1. Wipe off any labels and markers by KIMTECH-PURE wiper with methanol.

2. Scrub the inner wall by KIMTECH-PURE wiper; if still sticky, please use KIMTECH-PURE wiper with methanol.

3. Fill a 4-L glass beaker 3/4 full of mouth-up Teflonwares. Place a Teflon disc on the top of the Teflonwares for avoiding buoyancy problems, and place a watch glass on the top of the glass beaker.

4. Rinse all Teflonware together once with H_2O.

5. Fill the glass beaker with 1:1 Aqua Regia (1 Aqua Regia + 1 H_2O) over the top of Teflon disc. (1 Aqua Regia = 1 HNO_3+3 HCl; JT Baker RG) and leave in hood at room temperature over night.

6. Slowly boil the acid on a hotplate at 250℃ for 4-5 hours.

7. Turn off hotplate power, or if in use, remove the glass beaker onto a hot pad and cool the glass beaker for 30-60 minutes till it becomes warm and touchable.

8. Carefully pour the warm acid into an acid waste container in a sink.

9. Rinse all Teflonware with H_2O 3 times and empty into a sink with copious amounts of tap water.

10. Fill the glass beaker with H_2O with 50-100 ml ultrapure HCl (JT Baker RD) over the top of Teflon disc, and slowly boil the acid at 250℃ for 4-5 hours. Repeat steps 6-8.

11. Keeping the glass beaker in hood, remove watch glass and change gloves. For Teflon beaker, please go to step 12; for column and bottle, please jump to step 16.

12. Fill 9/10 full of 1% Aqua Regia (+ 0.005N HF) into each Teflon beaker and tightly close cap.

13. Place all Teflon beakers on a hotplate and reflux at 180℃ for 4-5 hours.

14. Turn off hotplate power, let the Teflon beakers cool for 15-20 minutes till them become warm and touchable.

15. Carefully open each Teflon beaker rinse it with copious amounts of tap water.

16. Dry items on KIMTECH-PURE wiper on a clean bench with class-100 air. After during, store them into personal container.
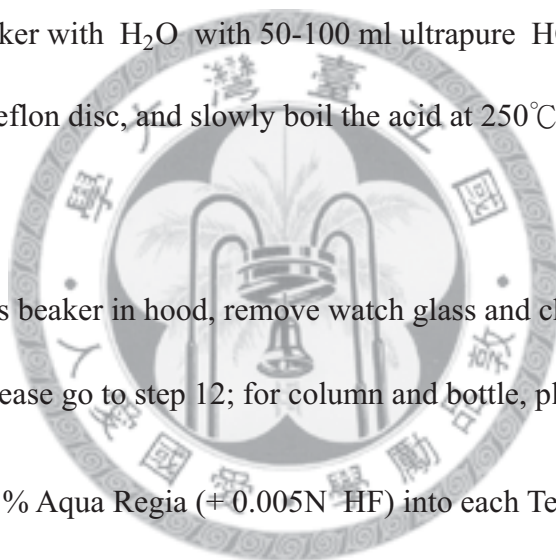
Plasticware (PP or PE bottle & centrifuge tube) – Method 1

1. Place a Teflon disc on the bottom of a 4L glass beaker and fill it 3/4 full of mouth-up Plasticware (bottle and centrifuge tube). Place a Teflon disc on the top of Plasticware to hold in place, and place a watch glass on the top of the glass beaker.

2. Rinse all Plasticware together once with H_2O.

3. Fill the glass beaker with 2.8 N HNO_3 (4 H_2O + 1 HNO_3; JT Baker RG) over top of Teflon disc, avoiding any buoyancy problems.

4. Slowly boil the acid on a hotplate at 240℃ for 4 hours.

5. Turn off hotplate power, or if in use, remove the glass beaker onto a hot pad and cool the glass beaker for 30-60 minutes till it becomes warm and touchable.

6. Carefully pour the warm acid into another 4L glass beaker for reusing or an acid waste container in a sink. (Acid can be used 2-3 times prior to discarding.)

7. Rinse all Teflonware with H_2O 3x and empty into sink with copious amounts of tap water.

8. Keeping the glass beaker in the hood, remove the watch glass and change gloves.

9. Rinse each item 3 times with H_2O and set on KIMTECH-PURE wiper mouth-down.

10. Dry the items on KIMTECH-PURE wiper on a clean bench with class-100 air. Put items into a storage container.

Plasticware (vials & pipette tips) – Method 2 (water bath)

1. Put plasticware into a 1L or a 2L PP bottle.

2. Rinse all Plasticware together once with H_2O.

3. Fill the container full with 2.8N HNO_3 (4 H_2O + 1 HNO_3; JT Baker RG) and tightly close the container.

4. With a Teflon disc on the bottom of a 4L glass beaker, put the container into it.

5. Fill H_2O into the glass beaker to 3 cm from top of the container and place a watch glass on the top.

6. Slowly boil the water on a hotplate at 240℃ for 4 hours.

7. Turn off the hotplate, or if in use, remove the glass beaker onto a hot pad and cool the glass beaker for 30-60 minutes till it becomes warm and touchable.

8. Carefully pour the warm acid from the container into another 4L glass beaker for reusing or a waste container in a sink. (Acid can be used 2-3 times prior to discarding.)

9. Fill the container 3/4 full with H_2O and pour into a sink with copious amounts of tap water twice for rinse.

10. Rinse each item 3 times with H_2O and set on KIMTECH-PURE wiper mouth-down.
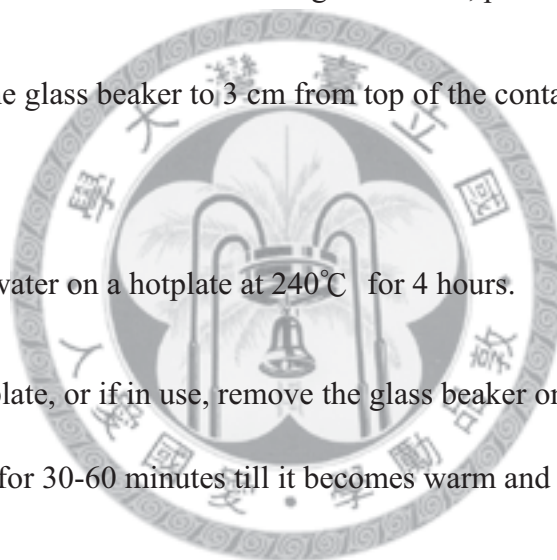
11. Dry the items on KIMTECH-PURE wiper on a clean bench with class-100 air. Put items into a storage container.

Plasticware (storage container & plastic rack) – Method 3

1. Rinse storage container or plastic rack with H_2O.

2. Soak storage container or plastic rack with dilute HNO_3 (20-50 ml HNO_3 in 1L H_2O; JT Baker RG) for 5-8 hours.

3. Wash item with H_2O and pour into sink with copious amounts of tap water.

4. Dry the items on KIMTECH-PURE wiper on clean bench with class-100 air.

Frit

1. Soak frits with 1:10 Aqua Regia (1 Aqua Regia + 10 H_2O) in a glass beaker and place a watch glass on the top. (1 Aqua Regia = 1 HNO_3+3 HCl; JT Baker RD)

2. Slowly boil the acid on a hotplate at 200℃ for 4-5 hours.

3. Turn off hotplate power, or if in use, remove the glass beaker onto a hot pad and cool the glass beaker for 30-60 minutes till it becomes warm and touchable.

4. Carefully pour the warm acid into a sink with copious amounts of tap water.

5. Rinse all frits together 3x with H_2O.

6. Soak frits with 2N HCl (Seastar) in a Teflon beaker for days; replace acid with another clean 2 N HCl; repeat this step 2-3 times. Clean frits with H2O and keep

them in the original beaker.

Appendix II   U-Th isotopic concentration data and dates

Sample ID	Weight g	^{238}U ppb	^{232}Th ppt	d^{234}U measured[a]	[^{230}Th/^{238}U] activity[c]	[^{230}Th/^{232}Th] ppm[d]	Age uncorrected	Age corrected[c,e,f]	d^{234}U$_{initial}$ corrected[b]	Age yr, BP[g]
YK5-01	0.1024	8730 ± 13	553.0 ± 7.1	215.8 ± 2.1	1.0192 ± 0.0024	265626 ± 3445	179,706 ± 1325	179,705 ± 1325	358.5 ± 3.7	179,643
YK5-02	0.1009	7335 ± 14	263.1 ± 7.0	218.4 ± 2.7	1.0235 ± 0.0027	471128 ± 12563	180,437 ± 1600	180,436 ± 1600	363.6 ± 4.8	180,375
YK5-05	0.1034	4322.4 ± 7.6	5997 ± 17	192.9 ± 2.3	1.0002 ± 0.0024	11903 ± 39	181,192 ± 1438	181,164 ± 1438	321.9 ± 4.1	181,102
YK5-07	0.1268	5041 ± 10	500.2 ± 5.7	187.7 ± 2.9	0.9997 ± 0.0026	166348 ± 1928	183,234 ± 1713	183,232 ± 1713	315.1 ± 5.0	183,171
YK5-08	0.1436	5729.6 ± 9.4	356.1 ± 5.1	184.6 ± 2.4	0.9986 ± 0.0027	265267 ± 3814	184,166 ± 1611	184,165 ± 1611	310.6 ± 4.2	184,103
YK5-09	0.1445	5375.3 ± 9.9	593.2 ± 5.0	202.1 ± 2.6	1.0161 ± 0.0022	152028 ± 1290	184,207 ± 1499	184,205 ± 1499	340.1 ± 4.7	184,143
YK5-10	0.1196	4986.2 ± 8.8	137.6 ± 5.8	201.6 ± 2.3	1.0175 ± 0.0023	608876 ± 25827	185,061 ± 1436	185,061 ± 1436	340.0 ± 4.1	184,999
YK5-13	0.1082	8808 ± 11	1103.7 ± 7.1	215.0 ± 1.9	1.0374 ± 0.0016	136699 ± 889	187,890 ± 1128	187,888 ± 1128	365.7 ± 3.5	187,826
YK5-14	0.1147	12100 ± 19	168.3 ± 6.1	210.0 ± 2.5	1.0368 ± 0.0027	1230671 ± 44610	189,876 ± 1694	189,876 ± 1694	359.2 ± 4.7	189,815
YK12-01	0.0298	6262.6 ± 4.1	3895 ± 24	309.6 ± 1.2	0.9620 ± 0.0015	25540 ± 164	133,762 ± 462	133,751 ± 462	451.8 ± 1.9	133,690
YK12-02	0.0422	5016.7 ± 2.5	12393 ± 25	296.1 ± 1.2	0.9590 ± 0.0017	6410 ± 17	135,884 ± 510	135,838 ± 511	434.7 ± 1.8	135,777
YK12-03	0.0337	6384.1 ± 3.6	1050 ± 21	296.2 ± 1.1	0.9796 ± 0.0014	98334 ± 1947	141,426 ± 463	141,423 ± 463	441.8 ± 1.7	141,362
YK12-04	0.0418	5675.3 ± 5.8	9675 ± 32	273.0 ± 1.6	0.9792 ± 0.0017	9483 ± 34	147,071 ± 670	147,039 ± 670	413.7 ± 2.6	146,978
YK12-05	0.0327	13314 ± 13	1488 ± 21	259.4 ± 1.5	0.9840 ± 0.0015	145382 ± 2094	152,201 ± 622	152,199 ± 622	398.9 ± 2.4	152,138

Sample ID	Weight g	^{238}U ppb	^{232}Th ppt	$d^{234}U$ measured[a]	$[^{230}Th/^{238}U]$ activity[c]	$[^{230}Th/^{232}Th]$ ppm[d]	Age uncorrected	Age corrected[c,e,f]	$d^{234}U_{initial}$ corrected[b]	Age yr, BP[g]
YK12-07	0.0292	11746.6 ± 5.5	1425 ± 24	253.54 ± 0.88	0.9852 ± 0.0013	134061 ± 2272	154,298 ± 485	154,296 ± 485	392.1 ± 1.5	154,235
YK12-08	0.0341	8830.3 ± 5.3	38573 ± 98	212.8 ± 1.2	0.9796 ± 0.0027	3702 ± 14	165,267 ± 1071	165,180 ± 1071	339.4 ± 2.2	165,120
YK12-09	0.0304	7106.6 ± 3.6	7546 ± 25	199.72 ± 0.88	0.9823 ± 0.0014	15274 ± 55	171,076 ± 643	171,054 ± 643	323.9 ± 1.5	170,993
YK12-10	0.0319	9513.1 ± 6.5	4483 ± 23	203.4 ± 1.1	0.9976 ± 0.0013	34954 ± 182	175,795 ± 717	175,786 ± 717	334.3 ± 2.0	175,725
YK12-11	0.0377	6109.1 ± 3.8	572 ± 18	178.4 ± 1.2	0.9875 ± 0.0013	174125 ± 5633	181,929 ± 770	181,927 ± 770	298.4 ± 2.1	181,866
YK23-02	0.0482	2893.2 ± 2.3	13899 ± 26	102.8 ± 1.5	0.8935 ± 0.0018	3070.9 ± 8.0	172,790 ± 1035	172,681 ± 1035	167.6 ± 2.4	172,620
YK23-03	0.0520	2608.9 ± 1.7	13210 ± 23	99.6 ± 1.1	0.9008 ± 0.0016	2937.3 ± 7.1	177,700 ± 946	177,585 ± 947	164.5 ± 1.9	177,525
YK23-04	0.0421	2705.2 ± 1.3	1370 ± 17	59.55 ± 0.91	0.8799 ± 0.0016	28683 ± 355	187,327 ± 1030	187,315 ± 1030	101.1 ± 1.6	187,254
YK23-05	0.0521	2541.1 ± 1.2	10313 ± 20	60.06 ± 0.85	0.8830 ± 0.0015	3592.3 ± 9.2	188,729 ± 982	188,632 ± 982	102.4 ± 1.5	188,571
YK23-06	0.0487	3255.5 ± 2.0	1365 ± 14	32.5 ± 1.1	0.8632 ± 0.0012	33986 ± 363	193,472 ± 994	193,462 ± 994	56.1 ± 1.8	193,401
YK23-07	0.0525	3084.7 ± 1.5	2354 ± 14	32.53 ± 0.90	0.8671 ± 0.0012	18764 ± 112	195,871 ± 932	195,852 ± 931	56.6 ± 1.6	195,791
YK23-08	0.0481	2208.7 ± 1.3	2343 ± 15	47.1 ± 1.0	0.8848 ± 0.0014	13768 ± 89	197,538 ± 1069	197,512 ± 1069	82.2 ± 1.8	197,451
YK23-10	0.0444	1917.04 ± 0.89	4503 ± 17	39.3 ± 1.1	0.8795 ± 0.0013	6182 ± 25	199,294 ± 1103	199,236 ± 1102	68.9 ± 1.9	199,175
YK23-11	0.0508	2720.4 ± 1.5	1128 ± 14	21.23 ± 0.94	0.8633 ± 0.0013	34369 ± 430	200,953 ± 1095	200,943 ± 1095	37.5 ± 1.7	200,882
YK23-13	0.0304	3355.3 ± 2.2	698 ± 23	16.2 ± 1.0	0.8657 ± 0.0014	68753 ± 2263	206,207 ± 1217	206,202 ± 1217	29.0 ± 1.8	206,141
YK23-14	0.0494	2262.6 ± 1.5	899 ± 19	15.0 ± 1.1	0.8655 ± 0.0015	35976 ± 777	206,922 ± 1340	206,900 ± 1340	26.9 ± 2.1	206,839
YK47-01	0.1088	765.96 ± 0.73	2997.5 ± 7.6	398.9 ± 1.8	1.0295 ± 0.0019	4343 ± 13	132,271 ± 565	132,205 ± 566	579.7 ± 2.8	132,144

71

Sample ID	Weight g	^{238}U ppb	^{232}Th ppt	d^{234}U measured[a]	[^{230}Th/^{238}U] activity[c]	[^{230}Th/^{232}Th] ppm[d]	Age uncorrected	Age corrected[c, e]	d^{234}U$_{initial}$ corrected[b]	Age yr, BP[f]
YK47-03	0.1050	812.37 ± 0.84	6437 ± 11	395.2 ± 1.8	1.0173 ± 0.0022	2120.0 ± 5.5	130,186 ± 610	130,052 ± 612	570.7 ± 2.8	129,991
YK47-05	0.1085	531.0 ± 2.0	18095 ± 59	428.9 ± 5.5	0.9502 ± 0.0058	460.4 ± 2.7	110,780 ± 1342	110,210 ± 1363	585.7 ± 7.8	110,148
YK47-06	0.0998	423.5 ± 1.5	18734 ± 63	458.1 ± 5.9	0.9606 ± 0.0062	358.6 ± 2.3	108,794 ± 1361	108,070 ± 1398	621.8 ± 8.3	108,009
YK47-07	0.1285	685.3 ± 2.7	2416.1 ± 8.5	439.4 ± 6.2	0.9131 ± 0.0040	4276 ± 17	102,655 ± 1040	102,596 ± 1039	587.2 ± 8.5	102,535
YK47-08	0.1003	885.7 ± 3.6	10672 ± 28	390.2 ± 6.6	0.7770 ± 0.0042	1064.8 ± 4.7	85,190 ± 924	84,976 ± 927	496.1 ± 8.5	84,915
YK47-09	0.1056	588.3 ± 1.5	1096.3 ± 7.3	397.3 ± 5.1	0.7420 ± 0.0023	6574 ± 45	79,138 ± 556	79,106 ± 556	496.8 ± 6.4	79,044
YK47-10	0.1042	244.41 ± 0.46	1797.8 ± 8.3	477.6 ± 2.9	0.7584 ± 0.0023	1702.3 ± 8.8	75,054 ± 380	74,931 ± 384	590.3 ± 3.6	74,870
YK61-01	0.0577	8647.5 ± 5.7	132 ± 12	314.3 ± 1.1	0.7989 ± 0.0010	862610 ± 78814	97,306 ± 224	97,306 ± 224	413.8 ± 1.4	97,244
YK61-02	0.0680	7297.3 ± 5.1	18922 ± 43	288.8 ± 1.2	0.8125 ± 0.0020	5174 ± 17	103,358 ± 445	103,308 ± 446	386.7 ± 1.6	103,247
YK61-04	0.0728	3427.4 ± 2.0	13736 ± 25	295.8 ± 1.2	0.9172 ± 0.0019	3779 ± 10	125,391 ± 512	125,316 ± 513	421.5 ± 1.8	125,255
YK61-05	0.0628	3636.8 ± 1.9	4502 ± 12	275.4 ± 1.2	0.9027 ± 0.0013	12039 ± 37	125,800 ± 410	125,777 ± 411	393.0 ± 1.8	125,715
YK61-06	0.0841	3974.8 ± 2.4	4663 ± 10	261.5 ± 1.2	0.8936 ± 0.0013	12577 ± 32	126,291 ± 408	126,268 ± 408	373.6 ± 1.8	126,207
YK61-07	0.0801	3418.6 ± 3.7	1271.0 ± 8.9	302.6 ± 1.8	0.9278 ± 0.0013	41205 ± 291	126,643 ± 476	126,636 ± 476	432.9 ± 2.6	126,575
YK61-08	0.0867	3040.1 ± 3.7	10628 ± 18	314.0 ± 2.1	0.9384 ± 0.0020	4432 ± 11	126,995 ± 640	126,931 ± 641	449.5 ± 3.1	126,870
YK61-09	0.0822	1755.9 ± 2.4	15029 ± 28	346.3 ± 2.0	0.9673 ± 0.0027	1866 ± 6	127,719 ± 731	127,567 ± 734	496.6 ± 3.1	127,506
YK61-10	0.0701	3030.6 ± 3.9	7146 ± 14	287.1 ± 2.2	0.9203 ± 0.0019	6444 ± 16	127,832 ± 635	127,788 ± 635	412.0 ± 3.2	127,727
YK61-11	0.0796	4454.4 ± 4.8	801.0 ± 8.8	313.7 ± 1.7	0.9452 ± 0.0013	86784 ± 959	128,698 ± 470	128,695 ± 470	451.4 ± 2.5	128,633

Sample ID	Weight g	^{238}U ppb	^{232}Th ppt	d^{234}U measured[a]	[^{230}Th/^{238}U] activity[c]	[^{230}Th/^{232}Th] ppm[d]	Age uncorrected	Age corrected[c,e]	d^{234}U$_{initial}$ corrected[b]	Age yr, BP[f]
YK61-12	0.0818	2434.4 ± 2.3	657.4 ± 8.6	314.5 ± 1.6	0.9479 ± 0.0012	57958 ± 756	129,212.8 ± 431	129,208 ± 431	453.1 ± 2.3	129,146
YK61-13	0.0999	3140.5 ± 3.0	132.3 ± 7.0	305.6 ± 1.6	0.9459 ± 0.0013	370865 ± 19563	130,517.7 ± 452	130,517 ± 452	441.9 ± 2.3	130,455
YK61-14	0.0852	5420.5 ± 6.6	3648 ± 10	306.2 ± 1.8	0.9502 ± 0.0016	23311 ± 67	131,466.3 ± 546	131,454 ± 546	443.9 ± 2.7	131,393
YK61-15	0.0879	2307.3 ± 1.8	1947.5 ± 8.3	303.9 ± 1.3	0.9801 ± 0.0012	19171 ± 84	139,776.2 ± 445	139,761 ± 445	451.0 ± 2.0	139,699
YK61-16	0.0830	5853.2 ± 7.4	3435 ± 11	287.2 ± 1.7	0.9743 ± 0.0017	27409 ± 90	142,086.6 ± 626	142,076 ± 626	429.2 ± 2.7	142,014
YK61-18	0.0892	6174.8 ± 8.5	405.3 ± 7.9	299.4 ± 2.0	1.0514 ± 0.0019	264459 ± 5140	162,164.9 ± 869	162,164 ± 869	473.5 ± 3.4	162,102
YK61-19	0.0955	4766.3 ± 5.3	347.8 ± 7.3	274.1 ± 1.7	1.0478 ± 0.0014	237115 ± 4998	169,055.9 ± 774	169,055 ± 774	441.9 ± 3.0	168,993
YK61-20	0.0781	2984.1 ± 2.9	1897.4 ± 9.4	239.0 ± 1.7	1.0238 ± 0.0015	26585 ± 135	172,561.1 ± 837	172,549 ± 837	389.2 ± 2.9	172,487

Analytical errors are 2s of the mean.

[a]d^{234}U = ([^{234}U/^{238}U]$_{activity}$ - 1) x 1000.

[b]d^{234}U$_{initial}$ corrected was calculated based on ^{230}Th age (T), i.e., d^{234}U$_{initial}$ = d^{234}U$_{measured}$ X e^{l234*T} , and T is corrected age.

[c][^{230}Th/^{238}U]$_{activity}$ = 1 - e^{-l230T} + (d^{234}U$_{measured}$/1000)[l$_{230}$/(l$_{230}$ - l$_{234}$)](1 - e$^{-(l230 - l234)T}$), where T is the age.

Decay constants are 9.1577 x 10^{-6} yr^{-1} for ^{230}Th, 2.8263 x 10^{-6} yr^{-1} for ^{234}U, and 1.55125 x 10^{-10} yr^{-1} for ^{238}U (Cheng et al., 2000).

[d]The degree of detrital ^{230}Th contamination is indicated by the [^{230}Th/^{232}Th] atomic ratio instead of the activity ratio.

[e]Isochron Ages.

[f]BP, the abbreviation of "before present," means the age before AD 1950.

Appendix III   Oxygen isotope records

YK05								
Depth (mm)	Age (kyr, BP)	δ¹⁸O (‰VPDB)	Depth (mm)	Age (kyr, BP)	δ¹⁸O (‰VPDB)	Depth (mm)	Age (kyr, BP)	δ¹⁸O (‰VPDB)
3.0	179.64	-7.782	75.0	182.79	-6.517	147.0	186.95	-7.868
6.0	179.75	-7.717	78.0	183.08	-7.454	150.0	187.18	-7.445
9.0	179.85	-8.200	81.0	183.38	-7.485	153.0	187.25	-7.644
12.0	179.96	-8.164	84.0	183.69	-7.358	156.0	187.33	-7.727
15.0	180.06	-7.685	87.0	184.00	-6.976	159.0	187.40	-7.453
18.0	180.17	-7.905	90.0	184.11	-7.701	162.0	187.47	-8.145
21.0	180.27	-8.073	93.0	184.12	-7.397	165.0	187.54	-7.573
24.0	180.37	-8.266	96.0	184.12	-7.426	168.0	187.61	-8.191
27.0	180.44	-7.940	99.0	184.13	-7.653	171.0	187.68	-7.592
30.0	180.51	-7.423	102.0	184.14	-7.429	174.0	187.75	-7.901
33.0	180.57	-7.885	105.0	184.21	-7.067	177.0	187.83	-7.512
36.0	180.64	-7.904	108.0	184.31	-7.293	180.0	188.37	-7.202
39.0	180.71	-7.402	111.0	184.42	-7.564	183.0	188.37	-7.194
42.0	180.77	-7.855	114.0	184.52	-7.700	186.0	188.37	-6.891
45.0	180.84	-7.538	117.0	184.62	-7.664	189.0	188.37	-6.731
48.0	180.90	-7.723	120.0	184.73	-7.295	191.0	188.37	-7.082
51.0	180.97	-7.750	123.0	184.83	-7.511			
54.0	181.04	-7.559	126.0	184.93	-8.183			
57.0	181.10	-7.139	129.0	185.10	-8.470			
60.0	181.38	-7.327	132.0	185.41	-8.133			
63.0	181.67	-7.183	135.0	185.72	-7.565			
66.0	181.95	-7.144	138.0	186.03	-7.420			
69.0	182.23	-7.586	141.0	186.34	-7.730			
72.0	182.51	-6.919	144.0	186.65	-8.510			

YK12								
Depth (mm)	**Age (kyr, BP)**	**δ¹⁸O (‰VPDB)**	**Depth (mm)**	**Age (kyr, BP)**	**δ¹⁸O (‰VPDB)**	**Depth (mm)**	**Age (kyr, BP)**	**δ¹⁸O (‰VPDB)**
3.0	133.52	-4.360	18.2	139.69	-7.431	33.7	144.47	-8.508
3.6	133.69	-4.631	18.8	139.97	-7.431	34.2	144.61	-8.033
4.2	133.86	-4.411	19.3	140.25	-7.850	34.8	144.76	-8.009
4.7	134.04	-4.591	19.9	140.52	-7.786	35.4	144.91	-8.153
5.3	134.21	-4.654	20.4	140.80	-7.680	36.0	145.06	-8.298
5.9	134.39	-5.081	21.0	141.08	-8.000	36.6	145.20	-8.335
6.5	134.56	-4.981	21.5	141.36	-7.809	37.1	145.35	-8.171
7.0	134.73	-4.857	22.1	141.51	-7.614	37.7	145.50	-8.837
7.6	134.91	-5.067	22.7	141.66	-8.033	38.3	145.65	-8.810
8.2	135.08	-4.633	23.2	141.81	-7.818	38.9	145.80	-9.419
8.8	135.26	-5.769	23.8	141.95	-7.920	39.4	145.94	-8.619
9.3	135.43	-5.562	24.4	142.10	-8.281	40.0	146.09	-8.279
9.9	135.60	-6.670	25.0	142.25	-7.850	40.6	146.24	-8.242
10.5	135.78	-4.976	25.6	142.40	-8.184	41.2	146.39	-8.665
11.1	136.06	-5.744	26.1	142.54	-8.060	41.8	146.54	-8.700
11.6	136.34	-6.066	26.7	142.69	-7.405	42.3	146.68	-8.468
12.2	136.62	-6.684	27.3	142.84	-7.870	42.9	146.83	-8.427
12.7	136.89	-7.253	27.9	142.99	-7.886	43.5	146.98	-9.207
13.3	137.17	-7.061	28.4	143.14	-8.251	44.1	147.19	-8.930
13.8	137.45	-6.684	29.0	143.28	-8.314	44.7	147.41	-8.616
14.4	137.73	-7.286	29.6	143.43	-7.934	45.3	147.62	-8.260
14.9	138.01	-6.938	30.2	143.58	-8.173	45.8	147.84	-8.590
15.5	138.29	-6.215	30.8	143.73	-8.396	46.4	148.05	-8.852
16.0	138.57	-6.701	31.3	143.87	-8.693	47.0	148.27	-7.610
16.6	138.85	-6.496	31.9	144.02	-8.294	47.6	148.48	-7.653
17.1	139.13	-7.130	32.5	144.17	-8.100	48.2	148.70	-7.868
17.7	139.41	-7.361	33.1	144.32	-8.916	48.8	148.91	-7.827

YK12								
Depth (mm)	**Age (kyr, BP)**	**δ¹⁸O (‰VPDB)**	**Depth (mm)**	**Age (kyr, BP)**	**δ¹⁸O (‰VPDB)**	**Depth (mm)**	**Age (kyr, BP)**	**δ¹⁸O (‰VPDB)**
49.3	149.13	-8.008	64.3	152.84	-8.074	79.0	164.63	-8.323
49.9	149.34	-7.963	64.8	152.89	-8.352	79.5	164.87	-9.416
50.5	149.56	-7.771	65.4	152.94	-8.337	80.0	165.12	-10.001
51.1	149.77	-7.775	65.9	153.00	-8.272	80.5	165.36	-10.719
51.7	149.99	-7.777	66.4	153.05	-8.049	81.0	165.36	-11.029
52.3	150.20	-7.020	66.9	153.11	-7.852	81.5	165.61	-11.181
52.8	150.42	-8.020	67.5	153.16	-8.083	82.0	165.85	-11.267
53.4	150.63	-7.939	68.0	153.21	-7.976	82.5	166.10	-10.671
54.0	150.85	-6.970	68.5	153.27	-8.032	83.0	166.34	-10.528
54.6	151.06	-7.910	69.0	153.32	-7.884	83.5	166.59	-10.231
55.2	151.28	-7.834	69.6	153.37	-8.012	84.0	166.83	-9.873
55.8	151.49	-8.097	70.1	153.43	-7.983	84.5	167.08	-9.769
56.3	151.71	-8.211	70.6	153.48	-8.114	85.0	167.32	-9.647
56.9	151.92	-8.030	71.1	153.54	-8.229	85.5	167.57	-9.263
57.5	152.14	-8.265	71.7	153.59	-8.375	86.0	167.81	-9.097
58.0	152.19	-8.758	72.2	153.64	-8.647	86.5	168.06	-9.964
58.5	152.25	-8.176	72.7	153.70	-8.552	87.0	168.30	-10.009
59.1	152.30	-7.905	73.2	153.75	-8.350	87.5	168.55	-9.447
59.6	152.35	-7.567	73.8	153.80	-8.401	88.0	168.79	-9.300
60.1	152.41	-7.664	74.3	153.86	-8.369	88.5	169.04	-9.580
60.6	152.46	-7.989	74.8	153.91	-8.507	89.0	169.28	-9.813
61.2	152.51	-7.900	75.3	153.97	-8.470	89.5	169.53	-9.885
61.7	152.57	-7.974	75.9	154.02	-8.443	90.0	169.77	-9.125
62.2	152.62	-7.838	76.4	154.07	-8.246	90.5	170.01	-10.395
62.7	152.68	-7.887	76.9	154.13	-8.292	91.0	170.26	-10.158
63.3	152.73	-7.930	77.4	154.18	-8.231	91.5	170.50	-10.312
63.8	152.78	-8.082	78.5	164.39	-8.759	92.0	170.99	-9.693

YK12						YK23		
Depth (mm)	Age (kyr, BP)	δ¹⁸O (‰VPDB)	Depth (mm)	Age (kyr, BP)	δ¹⁸O (‰VPDB)	Depth (mm)	Age (kyr, BP)	δ¹⁸O (‰VPDB)
92.6	171.29	-9.710	107.4	180.33	-7.231	2.4	172.62	-10.868
93.1	171.58	-9.954	107.9	180.71	-7.223	3.2	173.16	-10.301
93.7	171.88	-10.273	108.4	181.10	-7.418	4.0	173.71	-10.175
94.3	172.18	-10.196	109.0	181.48	-7.516	4.8	174.25	-10.017
94.8	172.47	-9.520	109.5	181.87	-7.223	5.6	174.80	-10.143
95.4	172.77	-9.855				6.4	175.34	-10.151
95.9	173.06	-9.960				7.2	175.89	-9.094
96.5	173.36	-10.009				8.0	176.43	-8.684
97.1	173.65	-10.440				8.8	176.98	-8.093
97.6	173.95	-10.255				9.6	177.52	-7.399
98.2	174.25	-10.015				10.4	186.96	-7.427
98.8	174.54	-9.261				11.2	187.25	-7.519
99.3	174.84	-9.499				12.0	187.55	-7.507
99.9	175.13	-9.491				12.8	187.84	-7.485
100.4	175.43	-9.386				13.6	188.13	-6.407
101.0	175.72	-9.637				14.4	188.42	-7.441
101.5	176.11	-9.462				15.2	188.72	-6.942
102.1	176.49	-9.671				16.0	193.22	-9.479
102.6	176.88	-9.248				16.8	193.40	-9.402
103.1	177.26	-7.936				17.6	193.58	-8.535
103.7	177.64	-8.146				18.4	193.76	-8.847
104.2	178.03	-6.522				19.2	193.93	-8.619
104.7	178.41	-6.209				20.0	194.11	-9.985
105.3	178.80	-7.569				20.8	194.29	-10.064
105.8	179.18	-7.375				21.6	194.46	-9.954
106.3	179.56	-7.247				22.4	194.64	-9.843
106.8	179.95	-7.163				23.2	194.82	-9.130

YK23								
Depth (mm)	Age (kyr, BP)	δ¹⁸O (‰$_{VPDB}$)	Depth (mm)	Age (kyr, BP)	δ¹⁸O (‰$_{VPDB}$)	Depth (mm)	Age (kyr, BP)	δ¹⁸O (‰$_{VPDB}$)
24.0	194.99	-10.022	46.0	201.70	-7.158	67.6	206.39	-6.253
24.8	195.17	-9.964	46.8	201.91	-6.645	68.4	206.42	-6.266
25.6	195.35	-9.843	47.6	202.13	-6.958	69.2	206.46	-6.452
26.4	195.53	-10.178	48.4	202.35	-7.081			
27.2	195.70	-10.203	49.2	202.56	-6.585			
28.0	195.87	-10.046	50.0	202.78	-6.402			
28.8	196.04	-9.842	50.8	203.00	-6.798			
29.6	196.21	-9.972	51.6	203.21	-6.843			
30.4	196.37	-10.374	52.4	203.43	-6.259			
31.2	196.54	-10.220	53.2	203.65	-6.154			
32.0	196.70	-9.934	54.0	203.86	-5.861			
32.8	196.87	-10.164	54.8	204.08	-6.539			
33.6	197.04	-10.173	55.6	204.30	-6.760			
34.4	197.20	-10.320	56.4	204.51	-6.633			
35.2	197.37	-9.851	57.2	204.73	-6.575			
36.0	197.55	-9.982	58.0	204.95	-6.779			
36.8	197.76	-10.008	58.8	205.17	-6.712			
37.6	197.96	-9.975	59.6	205.38	-6.893			
38.4	198.16	-9.634	60.4	205.60	-6.727			
39.2	198.36	-9.387	61.2	205.82	-7.018			
40.0	198.57	-9.528	62.0	206.03	-6.377			
40.8	198.77	-9.623	62.8	206.16	-6.065			
41.6	198.97	-9.662	63.6	206.20	-6.392			
42.8	200.83	-9.395	64.4	206.24	-6.606			
43.6	201.04	-9.272	65.2	206.27	-6.335			
44.4	201.26	-8.266	66.0	206.31	-6.471			
45.2	201.48	-7.060	66.8	206.35	-6.292			

YK47			YK61					
Depth (mm)	Age (kyr, BP)	$\delta^{18}O$ (‰$_{VPDB}$)	Depth (mm)	Age (kyr, BP)	$\delta^{18}O$ (‰$_{VPDB}$)	Depth (mm)	Age (kyr, BP)	$\delta^{18}O$ (‰$_{VPDB}$)
11.8	129.99	-6.620	0.5	95.44	-7.832	20.9	126.87	-8.066
12.8	130.11	-5.051	1.3	96.64	-8.257	21.6	127.05	-8.072
13.8	130.23	-5.687	2.0	97.84	-8.203	22.4	127.23	-7.381
14.8	130.35	-5.885	2.8	99.04	-8.512	23.1	127.41	-7.681
15.8	130.47	-5.932	3.5	100.24	-8.405	24.3	127.59	-7.280
16.8	130.59	-5.414	4.3	101.45	-8.627	25.0	127.68	-6.990
17.8	130.71	-5.462	5.0	102.65	-8.512	26.1	127.95	-5.597
18.8	130.83	-5.511	5.8	103.85	-8.562	26.9	128.18	-4.979
19.8	130.95	-6.020	6.5	102.65	-8.707	27.6	128.41	-4.625
20.8	131.07	-5.673	7.0	124.10	-8.749	28.4	128.63	-5.814
21.8	131.19	-6.097	7.8	124.26	-8.467	29.1	128.84	-5.468
22.8	131.31	-6.388	8.5	124.41	-8.260	29.9	129.04	-5.321
23.8	131.43	-5.406	9.3	124.56	-8.730	31.0	129.20	-5.398
24.8	131.55	-5.139	10.0	124.72	-8.991	31.8	129.26	-5.195
25.8	131.67	-5.004	10.8	124.87	-8.839	32.5	129.31	-5.547
26.8	131.79	-5.656	11.5	125.02	-8.502	33.3	129.37	-5.601
27.8	131.90	-5.213	12.3	125.18	-7.789	34.0	129.42	-5.579
28.8	132.02	-5.824	13.4	125.41	-8.711	34.8	129.48	-5.475
29.8	132.14	-5.866	14.1	125.56	-8.977	35.5	129.54	-5.325
			14.9	125.72	-9.006	36.3	129.59	-5.313
			15.6	125.96	-8.743	37.0	129.65	-5.215
			16.4	126.21	-9.049	37.8	129.70	-5.269
			17.1	126.30	-9.411	38.5	129.76	-5.309
			17.9	126.39	-8.831	39.3	129.81	-5.460
			18.6	126.48	-8.483	40.0	129.87	-5.693
			19.4	126.57	-7.861	40.8	129.93	-5.627
			20.1	126.72	-8.014	41.5	129.98	-5.726

YK61								
Depth (mm)	Age (kyr, BP)	δ¹⁸O (‰VPDB)	Depth (mm)	Age (kyr, BP)	δ¹⁸O (‰VPDB)	Depth (mm)	Age (kyr, BP)	δ¹⁸O (‰VPDB)
42.3	130.04	-5.996	62.5	131.50	-7.821	82.8	144.73	-8.913
43.0	130.09	-5.529	63.3	139.53	-7.834	83.5	144.97	-8.608
43.8	130.15	-5.365	64.0	139.70	-7.829	84.3	145.22	-8.424
44.5	130.20	-5.221	64.8	139.86	-8.131	85.0	145.46	-9.178
45.3	130.26	-4.903	65.5	140.03	-8.439	85.8	145.71	-9.931
46.0	130.32	-4.847	66.3	140.20	-7.880	86.5	145.96	-9.618
46.8	130.37	-5.061	67.0	140.36	-8.520	87.3	146.20	-8.015
47.5	130.43	-6.012	67.8	140.53	-8.656	88.0	146.45	-8.063
48.6	130.51	-5.702	68.5	140.69	-8.855	88.8	146.70	-7.838
49.4	130.56	-5.696	69.3	140.86	-8.983	89.5	146.94	-8.226
50.1	130.62	-5.798	70.0	141.02	-9.116	90.3	147.19	-8.150
50.9	130.67	-5.833	70.8	141.19	-9.163	91.0	147.44	-8.082
51.6	130.72	-5.372	71.5	141.35	-9.229	91.8	147.68	-7.959
52.4	130.78	-5.254	72.3	141.52	-8.929	92.5	147.93	-8.263
53.1	130.83	-5.465	73.0	141.68	-9.287	93.3	148.18	-8.752
53.9	130.88	-5.875	73.8	141.85	-9.034	94.0	148.42	-8.217
54.6	130.94	-5.678	74.5	142.01	-8.220	94.8	148.67	-7.914
55.4	130.99	-5.630	75.3	142.26	-8.381	95.5	148.92	-8.059
56.1	131.04	-5.449	76.0	142.51	-8.760	96.3	149.16	-8.188
56.9	131.10	-5.611	76.8	142.75	-8.889	97.0	149.41	-7.831
57.6	131.15	-5.774	77.5	143.00	-8.801	97.8	149.66	-8.441
58.4	131.21	-5.566	78.3	143.25	-8.990	98.5	149.90	-8.513
59.1	131.26	-5.719	79.0	143.49	-9.631	99.3	150.15	-7.949
59.9	131.31	-5.430	79.8	143.74	-9.427	100.0	150.39	-7.962
60.6	131.37	-5.519	80.5	143.99	-9.475	100.8	150.64	-8.296
61.4	131.42	-5.377	81.3	144.23	-9.469	101.5	150.89	-8.764
61.8	131.45	-6.989	82.0	144.48	-8.864	102.3	151.13	-8.156

YK61								
Depth (mm)	Age (kyr, BP)	δ¹⁸O (‰VPDB)	Depth (mm)	Age (kyr, BP)	δ¹⁸O (‰VPDB)	Depth (mm)	Age (kyr, BP)	δ¹⁸O (‰VPDB)
103.0	151.38	-7.793	123.3	158.04	-7.378	143.1	163.85	-8.437
103.8	151.63	-7.983	124.0	158.28	-6.919	143.9	164.02	-7.736
104.5	151.87	-8.222	124.8	158.53	-6.584	144.6	164.20	-7.386
105.3	152.12	-8.366	125.5	158.77	-6.707	145.4	164.37	-7.691
106.0	152.37	-8.200	126.3	159.02	-6.599	146.1	164.54	-8.823
106.8	152.61	-8.506	127.0	159.27	-7.043	146.9	164.72	-9.015
107.5	152.86	-8.481	127.8	159.51	-7.440	147.6	164.89	-8.456
108.3	153.11	-8.170	128.5	159.76	-7.995	148.4	165.07	-8.925
109.0	153.35	-8.428	129.3	160.01	-7.724	149.1	165.24	-9.502
109.8	153.60	-7.782	130.0	160.25	-7.768	149.9	165.42	-9.081
110.5	153.85	-8.284	130.8	160.50	-7.802	150.6	165.59	-8.777
111.3	154.09	-8.571	131.5	160.75	-7.967	151.4	165.77	-9.068
112.0	154.34	-7.870	132.3	160.99	-8.470	152.1	165.94	-9.278
112.8	154.58	-6.996	133.0	161.24	-8.617	152.9	166.11	-8.887
113.5	154.83	-8.139	133.8	161.49	-8.370	153.6	166.29	-9.183
114.3	155.08	-7.704	134.5	161.73	-8.090	154.4	166.46	-9.169
115.0	155.32	-7.144	135.3	161.98	-7.974	155.1	166.64	-9.428
115.8	155.57	-8.176	136.0	162.23	-8.161	155.9	166.81	-9.493
116.5	155.82	-8.266	136.4	162.28	-7.725	156.6	166.99	-9.601
117.3	156.06	-8.214	137.1	162.45	-7.248	157.4	167.16	-9.284
118.0	156.31	-8.136	137.9	162.63	-7.564	158.1	167.34	-9.792
118.8	156.56	-7.378	138.6	162.80	-7.598	158.9	167.51	-9.707
119.5	156.80	-6.232	139.4	162.97	-7.397	159.6	167.68	-10.246
120.3	157.05	-5.920	140.1	163.15	-7.233	160.4	167.86	-10.172
121.0	157.30	-6.369	140.9	163.32	-6.891	161.1	168.03	-9.935
121.8	157.54	-8.173	141.6	163.50	-7.988	161.9	168.21	-10.261
122.5	157.79	-7.233	142.4	163.67	-7.858	162.6	168.38	-10.564

YK61								
Depth (mm)	Age (kyr, BP)	δ¹⁸O (‰VPDB)	Depth (mm)	Age (kyr, BP)	δ¹⁸O (‰VPDB)	Depth (mm)	Age (kyr, BP)	δ¹⁸O (‰VPDB)
163.4	168.56	-10.297	183.3	172.42	-9.724			
164.1	168.73	-10.298	184.0	172.56	-9.998			
164.9	168.91	-9.919	184.4	172.63	-10.465			
165.6	169.08	-9.590	185.1	172.77	-10.266			
166.0	169.14	-9.950	185.9	172.92	-10.587			
166.8	169.28	-9.518	186.6	173.06	-10.629			
167.5	169.42	-9.818	188.1	173.34	-10.979			
168.3	169.56	-10.453	188.9	173.49	-11.040			
169.0	169.71	-9.800						
169.8	169.85	-9.362						
170.5	169.99	-9.883						
171.3	170.13	-10.327						
172.0	170.28	-10.268						
172.8	170.42	-9.615						
173.5	170.56	-10.562						
174.3	170.70	-11.557						
175.0	170.85	-10.682						
175.8	170.99	-10.484						
176.5	171.13	-11.000						
177.3	171.28	-11.138						
178.0	171.42	-11.291						
178.8	171.56	-11.161						
179.5	171.70	-10.673						
180.3	171.85	-10.421						
181.0	171.99	-10.267						
181.8	172.13	-9.808						
182.5	172.27	-9.659						